Mutations in *GANAB*, Encoding the Glucosidase IIα Subunit, Cause Autosomal-Dominant Polycystic Kidney and Liver Disease

Binu Porath,[1,16] Vladimir G. Gainullin,[1,16] Emilie Cornec-Le Gall,[1,2,3] Elizabeth K. Dillinger,[4] Christina M. Heyer,[1] Katharina Hopp,[1,5] Marie E. Edwards,[1] Charles D. Madsen,[1] Sarah R. Mauritz,[1] Carly J. Banks,[1] Saurabh Baheti,[6] Bharathi Reddy,[7] José Ignacio Herrero,[8,9,10] Jesús M. Bañales,[11] Marie C. Hogan,[1] Velibor Tasic,[12] Terry J. Watnick,[13] Arlene B. Chapman,[7] Cécile Vigneau,[14] Frédéric Lavainne,[15] Marie-Pierre Audrézet,[2] Claude Ferec,[2] Yannick Le Meur,[3] Vicente E. Torres,[1] Genkyst Study Group, HALT Progression of Polycystic Kidney Disease Group, Consortium for Radiologic Imaging Studies of Polycystic Kidney Disease, and Peter C. Harris[1,4,*]

Autosomal-dominant polycystic kidney disease (ADPKD) is a common, progressive, adult-onset disease that is an important cause of end-stage renal disease (ESRD), which requires transplantation or dialysis. Mutations in *PKD1* or *PKD2* (~85% and ~15% of resolved cases, respectively) are the known causes of ADPKD. Extrarenal manifestations include an increased level of intracranial aneurysms and polycystic liver disease (PLD), which can be severe and associated with significant morbidity. Autosomal-dominant PLD (ADPLD) with no or very few renal cysts is a separate disorder caused by *PRKCSH*, *SEC63*, or *LRP5* mutations. After screening, 7%–10% of ADPKD-affected and ~50% of ADPLD-affected families were genetically unresolved (GUR), suggesting further genetic heterogeneity of both disorders. Whole-exome sequencing of six GUR ADPKD-affected families identified one with a missense mutation in *GANAB*, encoding glucosidase II subunit α (GIIα). Because *PRKCSH* encodes GIIβ, *GANAB* is a strong ADPKD and ADPLD candidate gene. Sanger screening of 321 additional GUR families identified eight further likely mutations (six truncating), and a total of 20 affected individuals were identified in seven ADPKD- and two ADPLD-affected families. The phenotype was mild PKD and variable, including severe, PLD. Analysis of *GANAB*-null cells showed an absolute requirement of GIIα for maturation and surface and ciliary localization of the ADPKD proteins (PC1 and PC2), and reduced mature PC1 was seen in $GANAB^{+/-}$ cells. PC1 surface localization in $GANAB^{-/-}$ cells was rescued by wild-type, but not mutant, GIIα. Overall, we show that *GANAB* mutations cause ADPKD and ADPLD and that the cystogenesis is most likely driven by defects in PC1 maturation.

Introduction

Autosomal-dominant polycystic kidney disease (ADPKD) is one of the most common inherited disorders—it affects ~1/1,000 individuals worldwide—and is characterized by progressive cyst development and expansion in the kidneys.[1,2] In ~50% of affected individuals, ADPKD results in end-stage renal disease (ESRD), and 4%–10% of ESRD worldwide is due to ADPKD (see GeneReviews in Web Resources). ADPKD is caused by mutations in *PKD1* (MIM: 601313) or *PKD2* (MIM: 173910) (~85% and ~15% of mutation-resolved families, respectively).[3–6] Genotype-phenotype studies indicate an average age of 55.6 years for ESRD associated with truncating *PKD1* mutations, 67.9 years for non-truncating *PKD1* mutations, and 79.7 years for polycystic kidney disease 2 (PKD2 [MIM: 613095]).[7] Larger kidneys (measured by the height-adjusted, MRI-determined total kidney volume [htTKV]) and an earlier decline in renal function (measured by the estimated glomerular filtration rate [eGFR]) are also associated with PKD1 (MIM: 173900).[5,8] The PKD1- and PKD2-associated proteins, polycystin 1 (PC1) and 2 (PC2), respectively, are membrane glycoproteins with the primary cilium as a likely functional site.[9] PC1 is cleaved at the G-protein-coupled receptor proteolytic site (GPS), and this cleavage is essential for its function.[10,11] PC1 consists of two glycoforms of the N- and C-terminal (NT and CT, respectively) GPS-cleaved products: (1) mature, endoglycosidase H (EndoH) resistant (NTR and CTR) and (2) immature, EndoH sensitive (NTS and CTS).[12–14] The level of the mature glycoforms is associated with disease severity, and forming a complex

[1]Division of Nephrology and Hypertension, Mayo Clinic, Rochester, MN 55905, USA; [2]INSERM 1078, Department of Molecular Genetics, Université de Bretagne Occidentale, Brest, Brittany 29200, France; [3]Department of Nephrology, University Hospital, Brest, Brittany 29200, France; [4]Department of Biochemistry and Molecular Biology, Mayo Clinic, Rochester, MN 55905, USA; [5]Division of Renal Diseases and Hypertension, University of Colorado Denver, Aurora, CO 80202, USA; [6]Division of Biostatistics and Informatics, Mayo Clinic, Rochester, MN 55905, USA; [7]Section of Nephrology, University of Chicago, Chicago, IL 60637, USA; [8]Liver Unit, Clinica Universidad de Navarra, Pamplona, Navarra 31009, Spain; [9]Centro de Investigación Biomédica en Red de Enfermedades Hepáticas y Digestivas, Madrid 28029, Spain; [10]Instituto de Investigación Sanitaria de Navarra, Navarra 31008, Spain; [11]Department of Liver and Gastrointestinal Diseases, Biodonostia Health Research Institute, Donostia University Hospital, University of the Basque Country, Centro de Investigación Biomédica en Red de Enfermedades Hepáticas y Digestivas, Ikerbasque, San Sebastián 20014, Spain; [12]Department of Pediatric Nephrology, University Children's Hospital, Skopje 1010, Macedonia; [13]Division of Nephrology, School of Medicine, University of Maryland, Baltimore, MD 21201, USA; [14]Department of Nephrology, University Hospital, Rennes, Bretagne 35000, France; [15]Department of Nephrology, University Hospital, Nantes, Pays De La Loire 44000, France
[16]These authors contributed equally to this work
*Correspondence: harris.peter@mayo.edu
http://dx.doi.org/10.1016/j.ajhg.2016.05.004.

with PC2 is critical for PC1 maturation and surface and ciliary localization.[12,15,16]

In a number of comprehensive studies of the genes mutated in ADPKD, 7%–10% of families are genetically unresolved (GUR).[5–7,17] The typical finding of mild kidney disease in GUR cases[5] suggests that few such families are explained by missed, fully penetrant mutations at the complex, segmentally duplicated *PKD1* locus.[3,18] However, hypomorphic mutations at the existing loci—including those due to mosaicism,[19,20] phenocopies associated with autosomal-dominant tubulointerstitial kidney disease (ADTKD) loci,[21,22] and phenotypic and screening mistakes—most likely explain some unlinked and GUR families.[23] Nevertheless, additional genetic heterogeneity seems possible.

Subjects affected by ADPKD have a ~5× higher risk of developing intracranial aneurysms (ICAs).[24] However, polycystic liver disease (PLD) is the most frequent extrarenal complication in ADPKD; a minority of mainly females develop severe PLD that requires surgical intervention.[25,26] Unlike severe PKD, severe PLD is not associated with a particular genic or *PKD1* allelic type.[25] Isolated, autosomal-dominant PLD (ADPLD [MIM: 174050]) is a separate inherited disorder where severe PLD can also occur, but renal cysts are absent or very rare.[27] ADPLD is caused by mutations in *PRKCSH* (MIM: 177060), *SEC63* (MIM: 608648), or *LRP5*.[28–31] *PRKCSH* encodes the β subunit of glucosidase II (GIIβ);[32,33] GII is an endoplasmic-reticulum (ER)-resident enzyme that catalyzes hydrolysis of the middle and innermost glucose residues of peptide-bound oligosaccharides, and it triggers quality-control assessment of glycoprotein folding through the calnexin and calreticulin cycle.[34–39] SEC63 facilitates the translocation of secreted or membrane proteins across the ER membrane.[40–43] Induced loss of *Prkcsh* or *Sec63* in mouse kidneys results in PKD, and an interactive PC1-PC2 network with PC1 as the rate-limiting component has been proposed to maintain tubular differentiation.[13] This suggests that *PRKCSH* mutations might act through PC1 depletion, although PC2 reduction has also been noted with *Prkcsh* depletion or loss.[44,45] There is strong evidence of further genetic heterogeneity in ADPLD, given that only ~50% of cases have been explained by the known genes mutated in this disease.[27,46]

In this study, we employed global and focused screening of GUR ADPKD- and ADPLD-affected families to identify a gene mutated in these disorders. Characterization of cells null for this gene links the pathogenesis to the maturation and localization of PC1 and PC2.

Subjects and Methods

Sample and Data Collection and Clinical Analysis

The relevant institutional review boards and ethics committees approved all studies, and participants gave informed consent. Blood samples for DNA isolation were collected from the proband and all available family members and were isolated by standard methods by the Mayo Biospecimens Accessioning and Processing Core or the Genkyst study. Clinical and imaging data were obtained by review of clinical records. Total kidney volume (TKV) and total liver volume (TLV) were measured from clinical MRI and computed-tomography (CT) imaging at the Mayo Translational PKD Center, which employed the stereology method with Analyze software or a semi-automated approach,[47] and were adjusted for height (htTKV or htTLV). Enlarged kidneys or livers were defined as the mean + 2 SDs of the normal htTKV or htTLV adjusted for average height.[26,48] Kidney function was calculated from clinical serum creatinine measurements with the Chronic Kidney Disease Epidemiology Collaboration (CKD-EPI) formula in adults[49] and the Schwarz formula in the pediatric individual[50] and expressed as mL/min/1.73 m^2. Age at onset of high blood pressure was defined as when the affected individual started antihypertensive medication.

Whole-Exome Sequencing and Bioinformatics Analysis

Families were defined as GUR when no mutations were detected from Sanger sequencing or multiplex ligation-dependent probe amplification of *PKD1* and *PKD2*. In addition, the Genkyst cohort, including families PK20016, PK20017, and P1174, were screened for *HNF1B* (MIM: 189907) mutations, and families with a possible ADPLD diagnosis, including P1073, M472, and M656, were screened for *PRKCSH* and *SEC63* mutations.

Total genomic DNA was quantified with a Qubit 2.0 fluorometer (dsDNA BR Assay Kit, Thermo Fisher Scientific) and quality checked with a NanoDrop. Subsequently, 250 ng or 1 μg of DNA was sheared by sonication (Covaris E210, 150–200 bp) and purified by AMPure XP beads (Agencourt). The shearing efficiency was checked on a Agilent Bioanalyzer 2100 (DNA1000 assay). Whole-exome capture and Illumina library preparation were performed with the Agilent SureSelectXT Human All Exon V5+UTRs Kit on an Agilent Bravo workstation. The enriched library was sequenced with 101 bp paired-end reads on an Illumina HiSeq 2000 in the Mayo Medical Genome Facility. On average, three to four exomes per lane were multiplexed. Genome_GPS v.3.0.1 (Mayo Bioinformatics Core) was employed as a comprehensive secondary analysis pipeline for variant calling. In short, FASTQ files were aligned to the hg19 reference genome (UCSC Genome Browser) with Novoalign (V2.08.01) with the options -hdrhd off -v 120 -c 4 -i PE 425,80 -x 5 -r Random, and realignment and recalibration were performed with the Genome Analysis Toolkit (GATK) (3.3-0) Best Practices v.3 for each family separately. Overall, 75.6% of mapped reads aligned to the captured region, and 98.9% of the captured region was covered at 10× read depth. Multi-sample variant calling was performed with the GATK (3.3-0) Haplotype Caller, and variants were filtered with Variant Quality Score Recalibration for both SNVs and indels. Variant mining was performed with Golden Helix SNP & Variation Suite v.8 (SVS). All families were analyzed independently with the following filters: (1) quality filter of read depth ≥ 10× and genotype quality ≥ 20, (2) selection according to autosomal-dominant sample genotype pattern, (3) removal of Exome Aggregation Consortium (ExAC) Browser variants with a minor allele frequency > 0.1%, and (4) characterization of coding and non-coding SNVs within 14 bp of the splice site and subsequent removal of SNPs predicted to be neutral by one or more of six dbNSFP tools (SIFT, PolyPhen-2 HVAR, MutationTaster, Mutation Assessor,

FATHMM, and FATHMM MKL) and dbscSNV (removal of SNVs with Ada and RF scores < 0.6). Table S1 lists the variants that remained after the SVS analysis.

Sanger Sequencing and Mutation Validation

Primers to amplify the 25 exons of *GANAB* (GenBank: NM_198335.3), plus ~100 bp of flanking intervening sequences (IVSs), were designed with MacVector 12.0.6, and 50 ng of genomic DNA was used for PCR amplification (primers and PCR conditions are available upon request). Sanger sequencing was performed at Beckman Coulter Genomics according to standard approaches, and variants were identified with Mutation Surveyor software (SoftGenetics) and designated on the 25 exon *GANAB* isoform and corresponding protein (GenBank: NP_938149.2). When samples were available, segregation analysis was performed by sequence analysis of the mutated exonic fragment. Amino acid changes detected by Sanger sequencing were evaluated with the programs SIFT and Align GVGD, and the atypical splicing change in family M656 was evaluated with NNSPLICE 0.9 (Berkeley *Drosophila* Genome Project). The families affected by *GANAB* mutations originate from the US (M263, M641, 290100, M656, and M472), France (PK20016 and PK20017), Macedonia (P1174), and Spain (P1073). One family came from the HALT Progression of Polycystic Kidney Disease (HALT-PKD) cohort, two came from Genkyst, and the remainder came from the Mayo PKD Center population.

Using CRISPR/Cas9 to Generate Targeted *GANAB*-Mutated Cell Lines

Guide RNAs predicted to have the lowest off-targeting effect were cloned into pX330 (SpCas9) and verified by sequencing (see Table S2 for sequences). *GANAB* ex11-IVS12 was amplified by PCR (primer sequences are available on request), and the 550 bp genomic product was cloned into pCAG-EGxxFP[51] with restriction sites BamHI and EcoRI. Each gRNA was then co-transfected with p-CAG-EG-*GANAB*(11-IVS-12)-FP in renal cortical tubular epithelial (RCTE) cells and scored after 24 hr for EGFP-positive cells. gRNA4 was selected as the most efficient cutter and used for generating cell lines. pX330-gRNA4 was transfected into wild-type (WT) RCTE cells by electroporation, and the cells were allowed to recover for 36 hr prior to splitting and re-seeding as single-cell suspensions in a 96-well plate. Cells were grown for 10 days for the establishment of single clone cell colonies, split in half, and re-seeded for screening. Screening was performed with genomic DNA extraction followed by amplification using *GANAB* ex11-IVS12 primers and a subsequent T7 mismatch assay. For this assay, PCR amplicons were denatured at 95°C for 2 min and cooled gradually to 25°C at a rate of −2°C per second. The reaction mixture was then subjected to T7 endonuclease (T7E1, New England BioLabs) for 20 min at 37°C and visualized in 2% agarose gels. Clones were additionally screened by western blotting (WB) for the α subunit of glucosidase II (GIIα) and Sanger sequencing.

Generating FLAG-GIIα Constructs with Missense Variants

C-terminal Myc-DDK-tagged GIIα (isoform 3 [GenBank: NM_198335.3]) was obtained from OriGene. Missense mutations were introduced by site-directed mutagenesis with Q5 high-fidelity polymerase (New England BioLabs); primer sequences are shown in Table S3.

WB Studies, Glycosylation Analysis, and Immunoprecipitation

For purification of crude membrane protein, cells were grown to confluence, washed with Dulbecco's PBS (DPBS), scraped and reconstituted in LIS buffer (10 mM Tris HCl [pH 7.4], 2.5 mM $MgCl_2$, and 1mM EDTA) plus protease inhibitors (Complete, Roche), and incubated on ice for 15 min. Homogenized total membrane lysates were prepared by repeated passage through a 25.5G needle and centrifugation at 4,600 RPM for 5 min. All procedures employed pre-chilled containers and were performed in the cold room to minimize protein loss to degradation. For immunoprecipitation (IP), the pellet of crude membrane protein (75 mg) was solubilized in IP buffer, and samples were pre-cleared with blank A/G agarose for 2 hr. Antibodies to the C terminus of PC1 (PC1-CT) or PC2 (YCE2) were added overnight and then incubated with 50 mL of packed washed A/G Agarose (Thermo) for 2 hr. The agarose was washed three times in IP buffer and once in ice-cold H_2O, and the protein was eluted in either lithium dodecyl sulfate (LDS) plus tris(2-carboxyethyl)phosphine (TCEP) or agarose, split into three equal parts (untreated, EndoH, and PNGaseF), and subjected to deglycosylation analyses. Purified membrane protein and IP eluates were deglycosylated with EndoH and PNGaseF according to the manufacturer's (New England BioLabs) instructions. Twenty-five micrograms of input and 100% of the IP were loaded per SDS-PAGE lane.

Surface Glycoprotein Labeling and Immunoprecipitation

Surface glycoprotein labeling of living cells was performed as previously described.[15] Monolayer cells in 10 cm culture dishes were washed twice with ice-cold DPBS and then oxidized at 4°C in 1 mM NaIO4 containing DPBS (pH 7) for 30 min, quenched with ice-cold 1 mM glycerol in DPBS for 5 min, and washed twice with ice-cold DPBS. Oxime ligation was performed in the presence of 10 mM Aniline (Sigma-Aldrich) and 100 μM EZ-Link Alkoxyamine-PEG4-Biotin (Thermo Fisher Scientific) in 1% FBS supplemented with ice-cold DPBS buffer (pH 7.5) for 1 hr. Biotinylated cells were then washed three times in PBS and scraped. Reaction specificity was ensured with streptavidin-488 (Alexa Fluor) staining of a small sample of cells and visualized by fluorescent microscopy. Scraped cells were collected by centrifugation, subjected to purification of crude membrane protein, and solubilized in IP buffer (20 mM HEPES [pH 7.5], 137 mM NaCl, 1% NP-40, 10% (w/v) glycerol, 2 mM EDTA, and 2.5 mM $MgCl_2$) supplemented with protease inhibitors (Roche) for 15 min. Non-solubilized protein was removed by centrifugation and discarded. Neutravidin agarose was washed in IP buffer three times, and 50 mL of packed agarose was added to solubilized membrane protein and agitated at 4°C for 2 hr. Samples were washed three times in IP buffer and once in ice-cold H_2O. Protein was eluted in either LDS plus TCEP or agarose and subjected to deglycosylation analyses. Tris-acetate gels were washed with ultrapure water and stained with the ProteoSilver Silver Stain Kit (Sigma-Aldrich) according to the manufacturer's instructions.

Transfection, Confocal Microscopy, Immunofluorescence, and Surface PC1 Labeling

RCTE cells were split at a ratio of 1:2 the day before electroporation and transfected at ~80% confluency. Electroporation of RCTE cells was performed with the Bio-Rad Gene Pulser with a square-wave protocol: 110V, 25 ms pulse and 0.2 cm cuvettes (Bio-Rad) in

electroporation buffer (20 mM HEPES, 135 mM KCl, 2 mM $MgCl_2$, and 0.5% Ficoll 400 [pH 7.6]). TagGFP-PC2 and mCherry-PC1 used in this study have been previously described.[15] RCTE cells were grown on glass coverslips, washed once with DPBS, fixed in 3.5% paraformaldehyde (PF) for 30 min, permeabilized with 0.1% Triton in DPBS (pH 7.5), washed again in PBS, and incubated in blocking buffer (10% normal goat serum, 1% BSA, and 0.1% Tween in PBS [pH 7.5]) for 30 min. After three PBS washes, primary antibodies were added to IF buffer (1% BSA, PBS [pH 7.5], and 0.1% Tween) for 2 hr at room temperature or overnight at 4°C with gentle agitation. After three PBS washes, conjugated secondary antibody (AlexaFluor, Invitrogen) was added for 1 hr. DAPI was added for 1 min to stain nuclei.

For surface labeling of mCherry-PC1, transfected RCTE cells were cooled at 4°C for 15 min, washed once in ice-cold PBS and pre-chilled mCherry antibody (BioVision), and incubated in 0.5% BSA in PBS for 30 min at 4°C. Cells were then fixed in 3.5% PF, and conjugated secondary antibody was added to IF buffer for 30 min. Confocal microscopy was performed with a Zeiss Axiovert equipped with Apotome.

For pH shift and SDS IF, the fixation and antigen-retrieval method was performed for visualizing endogenous PC2 in MEFs. For partially denaturing the protein, cells were grown to 100% confluency and serum starved for 48 hr, fixed in 3% PF (pH 7.5) for 15 min, fixed in 4% PF (pH 11]) in 100 mM borate buffer for 15 min, and then permeabilized in 5% SDS for 5 min. Subsequently, PC2 antibody (H280) staining was performed overnight at a 1:200 dilution at 4°C as described above.

Antibodies

The following antibodies were used: PC1-NT, 7e12[52] (N-terminal, mouse monoclonal; 1/1,000 for WB); PC1-CT, EB08670 (C-terminal, goat; Everest Biotech; 1/250 for IP); PC2, H280 (rabbit; Santa Cruz; 1/5,000 for WB and 1/200 for IF); PC2, YCE2 (mouse monoclonal; Santa Cruz; 1/2,000 for WB and 1/500 for IF); EGFR (rabbit; BD Transduction labs; 1/1,000 for WB); acetylated α-tubulin (Invitrogen; 1/5,000 for IF); mCherry, 5993-100 (rabbit; BioVision; 1/1,000 for surface labeling); FLAG M2 (Sigma; 1/1,000 for IF); and GIIα, ab179805 (Abcam; 1/2,000 for WB).

Results

WES Identifies *GANAB* as a Gene Mutated in ADPKD

After *PKD1* and *PKD2* mutation analysis for base-pair and larger rearrangements, we identified 327 GUR families out of ~3,600 screened. These GUR families originated from the HALT-PKD cohort (64) (an ADPKD clinical trial) and the Consortium for Radiologic Imaging Studies of Polycystic Kidney Disease (CRISP) (16) and Genkyst (124) ADPKD observational studies. In addition, 123 Mayo PKD Center GUR families affected by ADPKD or mild renal cystic disease and PLD were included. Although a firm clinical diagnosis of ADPKD was made in 247 GUR pedigrees, in 80 pedigrees the disease presentation was more atypical (cystic kidney disease without kidney enlargement), although the vast majority exceeded the defined ultrasound or MRI criteria for an ADPKD diagnosis.[53,54] In the seven remaining families, the disease presentation was more consistent with ADPLD, although all but one had some renal cysts. *PRKCSH* and *SEC63* screening was also performed in these families before inclusion. Six multiplex GUR ADPKD-affected families were screened by WES, and standard screening methods were employed to identify mutated, dominant genes (see Subjects and Methods); the detected genes and variants are listed in Table S1. A missed *PKD1* mutation was identified in one family (M560).

From this WES analysis, one candidate gene, *GANAB*, encoding the catalytic subunit of glucosidase II (GIIα), appeared most promising given that *PRKCSH* encodes the non-catalytic β subunit of this enzyme, and mutations in this gene cause ADPLD. *GANAB* (in chromosomal region 11q12.3; genomic size 21.9 kb) has two splice forms shown by in silico and RT-PCR analysis to be approximately equally expressed in the human kidneys and liver (Figure S1): isoform 3 (GenBank: NM_198335.3) has 966 aa (~110 kDa), 25 exons, and 2,898 bp of coding sequence, and isoform 2 (GenBank: NM_198334.2) has 944 aa (~107 kDa), 24 exons (in-frame skipping of exon 6), and 2,832 bp of coding sequence.[36,38] We employed the larger splice form for mutation screening and designation and functional studies. ExAC Browser exome data (60,706 individuals) list five loss-of-function (LoF) *GANAB* mutations out of an expected 49.7 (probability of LoF intolerance [pLI] = 1.0; see Subjects and Methods), a figure similar to that for *PKD2* (7/37.6; pLI = 1.0) and consistent with *GANAB* mutations' causing dominant disease.[55,56]

The *GANAB* missense variant, c.1265G>T (p.Arg422Leu), was detected by WES in family M263 and found in the affected father and daughter, but not the unaffected daughter (Figures 1A–1C). In silico analysis, including conservation in multi-sequence alignments (MSAs) of proteins orthologous to yeast and related glucosidases showed that this variant is highly predicted to be pathogenic (Figures 1D and 1E). Both of the affected individuals had mild kidney and significant liver cystic disease (Figures 1F and 1G and Table 1).

Identification of Further ADPKD-Affected Families with *GANAB* Mutations

Given that mutations in *GANAB* might account for disease in families with unresolved ADPKD, we analyzed our remaining GUR cohort of 321 families by Sanger sequencing of the coding region. From this analysis, we identified eight additional families affected by *GANAB* mutations: three frameshift, two splicing, one nonsense, and two missense mutations (Table 1). Data from the ExAC Browser showed that none of the *GANAB* variants, except c.152_153delGA (reported once), have been reported in the 60,706 unrelated individuals sequenced as part of various disease-specific and population genetic studies.[55] Additionally, none of these variants were seen in the NHLBI Exome Sequence Project (ESP) Exome Variant Server.

The *GANAB* frameshift mutation, c.1914_1915delAG (p.Asp640Glnfs*77), was found in two families, M641 and 290100 (Figures 2A–2E, Figures S2A, S2B, and S3A, and Table 1). In M641, two sisters had relatively mild

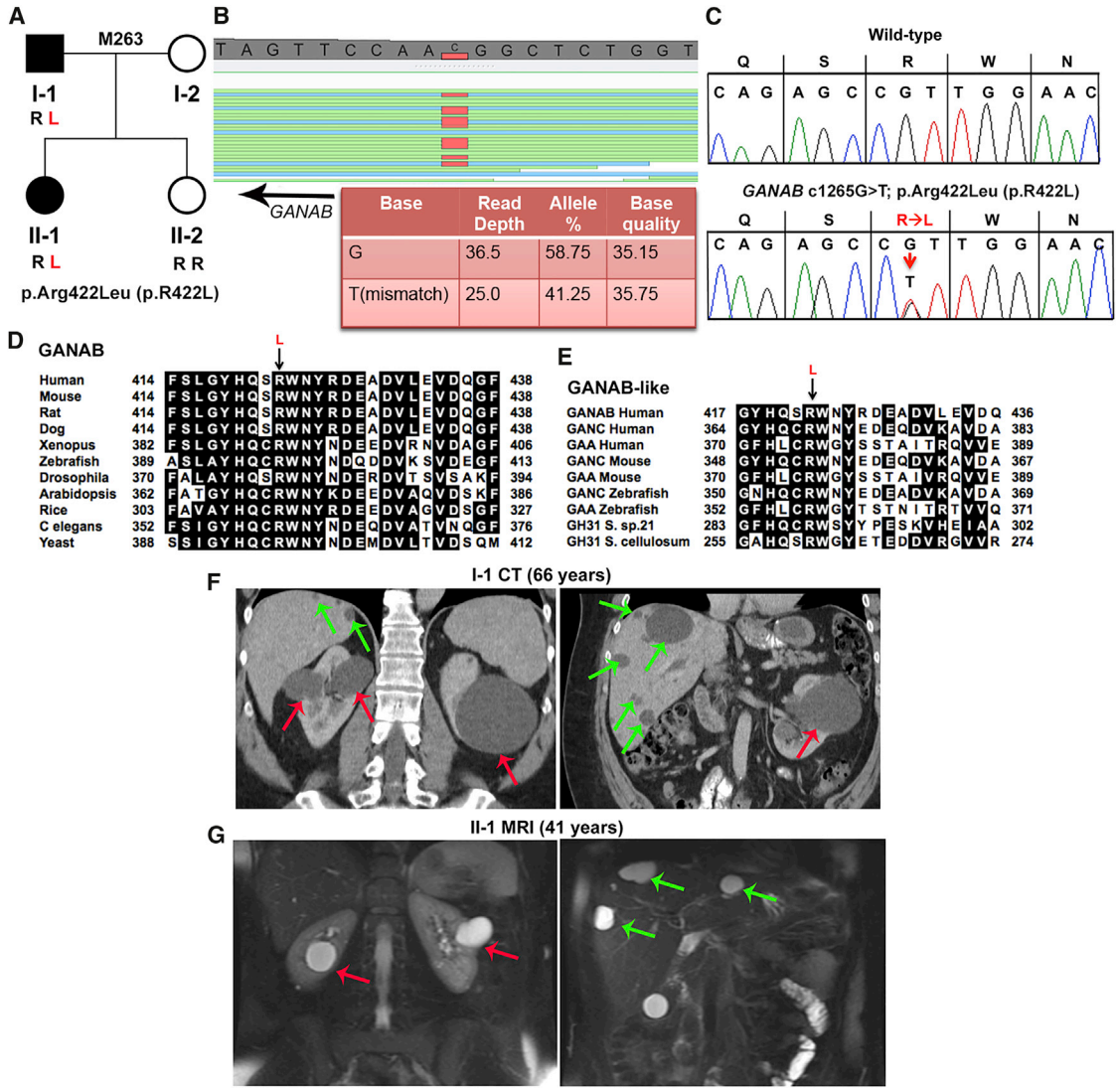

Figure 1. WES Analysis Reveals GIIα p.Arg422Leu (c.1265G>T) in Family M263 as the Likely Pathogenic Variant

(A) Pedigree of family M263 shows that the two affected individuals (I-1 and II-1, shaded in black) have the GIIα p.Arg422Leu (p.R422L) missense variant resulting from c.1256G>T in exon 12, but the unaffected daughter (II-2, for whom no cysts were detected on ultrasound at 30 years of age) does not.

(B) GenomeBrowse (SVS, Golden Helix) view of the WES results from II-1 show *GANAB* variant c.1265G>T (reverse strand), and details of the reads are tabulated below.

(C) Sanger sequencing confirmation of heterozygous GIIα variant p.Arg422Leu (p.R422L) (c.1256G>T) in II-1. The WT is shown for comparison.

(D) MSA of GIIα orthologous proteins shows invariance of Arg422 from humans to yeast. In silico analysis of the likely pathogenicity of GIIα p.Arg422Leu (p.R422L) shows variant scores (SIFT = 0.00, Align GVGD = C65) characteristic of a highly likely pathogenic mutation.

(E) MSA of related glucosidases GANC (neutral alpha-glucosidase C) and GAA (lysosomal alpha-glucosidase) of various eukaryotic species and prokaryotic GH31 (glycosyl hydrolase family 31) shows invariant conservation of GIIα Arg422.

(F) CT scan with contrast of kidneys and liver of individual I-1 at 66 years shows a few large kidney cysts (red arrows) and multiple scattered liver cysts (green arrows).

(G) T2-weighted MRI of II-1 at 41 years shows a few kidney (red arrows) and liver (green arrows) cysts.

PKD with variable liver cysts. The family history was unclear: the father died at 75 years with renal cell cancer but no reported cysts, and there was no information on the mother. Both sisters had ICAs (see the Figure 2 legend for details), and the father was reported to have a ruptured aneurysm. In family 290100, the father and son both had mild PKD, and multiple liver cysts were present in the father, but not the son.

In family P1174, the *GANAB* missense variant, c.1214C>G (p.Thr405Arg), was found in three generations, including in individual III-1, in whom renal cysts were detected incidentally in infancy (Figures 2F–2H, Figures S2C and S3B, and Table 1). The substituted residue is invariant in orthologs and conserved in related proteins (Figures 2I and 2J). The *GANAB* splicing mutation, c.2690+2_+7del, was found in four affected family

Table 1. Clinical Presentation of Kidney and Liver Disease in the 20 Affected Individuals from Nine Families with *GANAB* Mutations

						Radiologic Presentation							
						Kidneys					Liver		
Family	*GANAB* Mutation	Subject	Sex	eGFR[a] (Age in Years)	HBP (Age in Years[b])	Type	Age[c]	Cysts	Volume[d]	Figure	Cysts	Volume[e]	Figure
M263[f]	c.1265G>T (p.Arg422Leu)	I-1	M	78 (66)	N (67)	CT	66	~10 bilateral cysts (largest 11 cm)	302[g]	1F	>50 scattered cysts (largest 6 cm)	1,226	1F
		II-1	F	91 (42)	N (43)	MRI	41	~10 bilateral cysts (largest 3 cm)	211	1G	>20 scattered cysts (largest 3 cm)	835	1G
M641	c.1914_1915delAG (p.Asp640Glnfs*77)	II-1	F	86 (51)	Y (40)	CT	55	~15 bilateral cysts (largest 10 cm)	822[g]	S3A	no liver cysts detected	1,505[h]	S3A
		II-2	F	104 (46)	N (50)	CT	45	~10 bilateral cysts (largest 6 cm)	318[g]	2B	~20 scattered cysts (largest 2 cm)	764	2B
290100	c.1914_1915delAG (p.Asp640Glnfs*77)	I-1	M	78 (65)	N (65)	MRI	58	~8 bilateral cysts (largest 2 cm)	227	2E	>30 scattered cysts (largest 3 cm)	1,255	2E
		II-1	M	87 (25)	Y (13)	MRI	24	~12 bilateral cysts (largest 2.5 cm)	259	2D	none	832	2D
P1174	c.1214C>G (p.Thr405Arg)	I-1	M	NA[i]	N (61)	US	55	3 cysts in the left kidney	NE	S3B	1 cyst (1.5 cm)	NE	–
		II-1	F	NA[i]	N (35)	US	29	2 cysts in the right kidney	NE	2H	NA	NA	–
		III-1	M	122 (9)	N (9)	MRI	9	~5 bilateral cysts (largest 2 cm)	116	2G	none	492	–
M656	c.2690+2_+7del	I-1	M	NA[i]	Y (55)	CT*	67	multiple small cysts	NE	S3C	none	NE	S3C
		II-1	M	84 (39)	N (39)	US	44	multiple cysts reported	NA	–	multiple cysts reported	NA	–
		II-2	F	77 (50)	N (50)	US	52	~5–10 bilateral cysts (largest 2 cm)	NE	S3D	>20 scattered cysts (largest 5 cm)	NE	S3D
		II-3	M	95 (49)	Y (35)	MRI	43	>30 bilateral cysts (largest 3 cm)	SE	2L	>20 scattered cysts (largest 1 cm)	NE	2L
PK20016	c.39−1G>C	II-1	M	90 (53)	Y (45)	CT*	52	~20 bilateral cysts (largest 10 cm)	665[g]	3B	~20 scattered cysts (largest 2 cm)	1,449[h]	3B
PK20017	c.2176C>T (p.Arg726*)	II-1	F	77 (78)	Y (53)	US	78	~40 bilateral cysts (largest 3 cm)	NE	3D	~20 scattered cysts (largest 1.5 cm)	NA	3D
P1073	c.2515C>T (p.Arg839Trp)	I-2	F	NA	NA	US	(78)	unknown	NA	–	multiple cysts reported	NA	–
		II-1	F	86 (50)	N	CT*	43	~8 bilateral cysts (largest 1 cm)	196	3F	severe PLD, transplant at 43 years	4,641[h]	3F
		II-2	M	NA	NA	US	(44)	unknown	NA	–	multiple cysts reported	NA	–

(*Continued on next page*)

Table 1. *Continued*

Family	*GANAB* Mutation	Subject	Sex	eGFR[a] (Age in Years)	HBP (Age in Years[b])	Radiologic Presentation							
						Kidneys					Liver		
						Type	Age[c]	Cysts	Volume[d]	Figure	Cysts	Volume[e]	Figure
M472	c.152_153delGA (p.Arg51Lysfs*21)	II-1	F	82 (58)	N (58)	MRI	58	~20 cysts (largest 1 cm)	223	3I	severe PLD, resections at 47 and 48 years	1,749[f,h]	3I
		II-2[k]	F	NA	N (50)	MRI	50	~16 bilateral cysts (largest 6 cm)	305[g]	S3E	>50 scattered cysts (largest 5 cm)	1,249[h]	S3E

Abbreviations are as follows: CT, computed tomography; CT*, contrast-enhanced CT; eGFR, estimated glomerular filtration rate; HBP, high blood pressure; N, no; NA, not available; NE, not enlarged; SE, slightly enlarged; US, ultrasound; and Y, yes.
[a]Expressed in mL/min/1.73 m^2 on the basis of the last data available; obtained with the CKD-EPI formula in adults[49] and the Schwarz formula in the pediatric individual.[50]
[b]Age at HBP diagnosis or blood-pressure measurement.
[c]Age at imaging examination. Values in parentheses are the present age if images are not available.
[d]Kidney volume measurement or estimate (NE or SE). Values are the measured height-adjusted total kidney volume (htTKV) in mL/m.
[e]Liver volume measurement or estimate (NE). Values are the measured height-adjusted total liver volume (htTLV) in mL/m.
[f]The mutation in this pedigree was first identified by whole-exome sequencing.
[g]Enlarged values: mean + 2 SDs of normal male and female htTKV.[48]
[h]Enlarged values: mean + 2 SDs of normal male and female htTLV.[26]
[i]Kidney function was reported to be within the normal range.
[j]htTLV after resections.
[k]A sample was unavailable, and so the *GANAB* mutation was not confirmed.

members in M656 (Figures 2K and 2L, Figures S2D, S3C, and S3D, and Table 1). All members (apart from II-3, who had multiple kidney cysts) had no to mild cystic liver disease and mild kidney disease. Of note, the mother (without the *GANAB* mutation) had multiple cysts of unresolved etiology. PK20016 had the splicing mutation c.39−1G>C, and PK20017 had the nonsense mutation c.2176C>T (p.Arg726*), and both had only one known affected family member (Figures 3A–3D, Figures S2E and S2F, Table 1). Both individuals had multiple kidney cysts and a few liver cysts.

Identification of Families Affected by *GANAB* Mutations and ADPLD

Unlike the described ADPKD-affected families, families P1073 and M472 had a possible diagnosis of ADPLD, although a few renal cysts were present. P1073 had the missense mutation c.2515C>T (p.Arg839Trp), which is at an invariant site in orthologs and segregates in three affected family members (Figures 3E–3G, Figure S2G, and Table 1). As indicated, there were very few renal cysts but multiple liver cysts, and the daughter (II-1) required a liver transplant at 43 years. M472 individual II-1, who had the *GANAB* frameshift mutation c.152_153delGA (p.Arg51Lysfs*21) (Figures 3H and 3I, Figure S2H, and Table 1), had a few small kidney cysts but severe PLD that required partial liver resections. A similar phenotype with less severe PLD was seen in II-2 (Figure S3E), although a sample was unavailable for mutation analysis.

Characterization of the Effect of *GANAB* Loss on PC1 and PC2 Maturation and Localization

From the genetic studies, mutations in *GANAB* were shown to be a cause of ADPKD and ADPLD, so we next explored the mechanism of pathogenesis by cellular analysis. CRISPR/Cas9 targeting of *GANAB* exon 12 in human RCTE cells generated clones with biallelic frameshift mutations (null; clone C6) or a single in-frame deletion (heterozygous; E4) (Figures S4A–S4D). Analysis of the polycystin complex immunocaptured with PC2 or PC1-CT antibodies in $GANAB^{-/-}$ cells showed that the PC1 N-terminal, mature product (PC1-NTR) was absent (Figures 4A and 4B). In contrast, full-length (GPS-uncleaved) PC1, PC1-NTS, and PC2 were elevated, indicating that GIIα plays a major role in PC1 maturation. We previously showed an interdependence of PC1 and PC2 for localization, including to cilia,[15] and so to assess localization of the polycystin complex, we analyzed PC2. Ciliary localization of PC2 was completely absent in $GANAB^{-/-}$ cells, although cilia formed normally (Figure 4C and Figure S4E).[15,16] Given that affected individuals harbored just one *GANAB* mutation, we assayed $GANAB^{+/-}$ cells and found a proportional, ~50%, depletion of PC1-NTR (Figures 4D and 4E). Analysis of the maturation of other membrane proteins (epidermal growth factor receptor [EGFR] and E-cadherin) showed that they were not

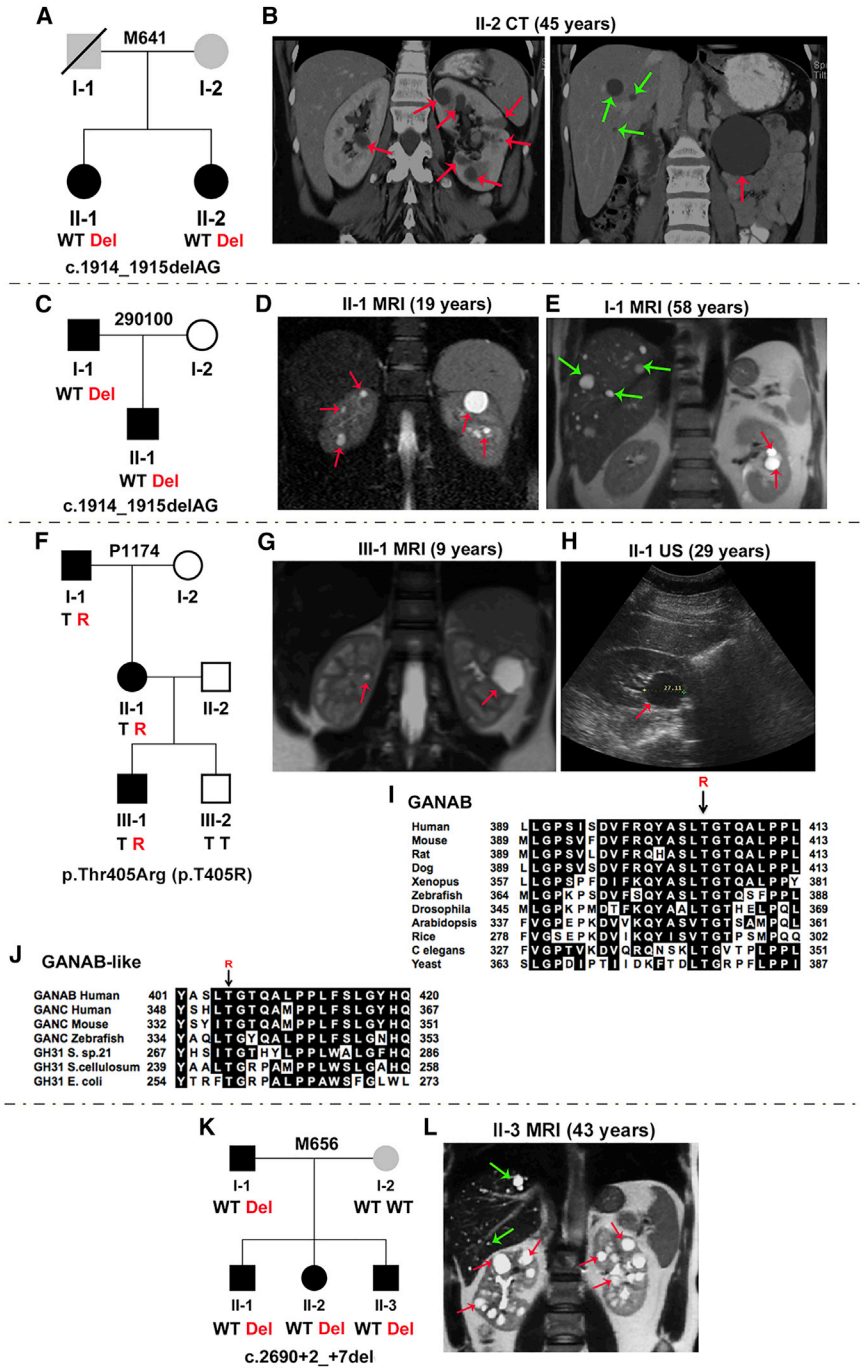

Figure 2. Characterization of *GANAB* Mutations in Four ADPKD-Affected Families

(A) Pedigree of family M641 shows c.1914_1915delAG (p.Asp640Glnfs*77) (exon 17) in two affected siblings. Both sisters had basilar tip aneurysms, and II-2 also had two aneurysms detected on the left middle cerebral artery. The affected status of the parents is unclear (gray shading); I-1 had renal cell carcinoma and a ruptured aneurysm, but no reported PKD.

(B) CT scan of kidneys and liver from II-2 shows multiple kidney and occasional liver cysts.

(C) Pedigree of family 290100 shows c.1914_1915delAG in the father and son.

(D and E) MRI shows a few kidney but no hepatic cysts in II-1 (D) and a few kidney and scattered liver cysts in I-1 (E).

(F) Pedigree of family P1174 shows p.Thr405Arg (p.T405R) (c.1214C>G, exon 11) in three affected individuals; III-2, for whom no cysts were detected by ultrasound at 5 years, did not have the variant.

(G and H) MRI of III-1 shows bilateral kidney cysts (G), and ultrasound (US) of II-1 shows a single large renal cyst (H).

(I) MSA of GIIα orthologs shows that Thr405 is invariant across species. In silico mutation analysis highly predicts p.Thr405Arg (p.T405R) to be pathogenic (SIFT = 0.00, Align GVGD = C65).

(J) MSA of GANAB-like proteins shows invariant conservation of this residue.

(K) Pedigree of family M656 shows c.2690+2_+7del (IVS20) in four affected members. Splicing predictions show complete loss of the donor site. The mother (I-2), who does not have the *GANAB* mutation, has ~5 kidney and ~30 liver cysts, but no detected *PKD1*, *PKD2*, *PRKCSH*, or *SEC63* mutations.

(L) MRI of II-3 shows small hepatic and multiple renal cysts. Red and green arrows indicate kidney and liver cysts, respectively. Where multiple cysts are present, only representative cysts are highlighted.

(or only mildly) affected by loss of GIIα (Figure 4A). Further analysis of terminally glycosylated proteins in *GANAB*$^{-/-}$ cells did not suggest a global disruption of surface-localized proteins (Figures S4F–S4H).

Functional Analysis of *GANAB* Mutations and Variants

To determine the effect of *GANAB* loss on PC1 localization by immunofluorescence and to test the pathogenicity of detected GIIα variants, we co-transfected WT and *GANAB*$^{-/-}$ cells with tagged PC1 and PC2 constructs (mCherry-PC1-V5 and GFP-PC2; Figures 5A and 5B).[15] GIIα loss prevented efficient surface localization of tagged PC1, which was restored by co-expression of WT FLAG-GIIα (Figure 5A). Identified GIIα missense variants (p.Thr405Arg, p.Arg422Leu, and p.Arg839Trp), expressed as FLAG-GIIα constructs, failed to rescue PC1 surface localization in *GANAB*$^{-/-}$ cells (Figure 5A), whereas three other variants considered likely to be neutral (c.284A>G [p.Gln95Arg], c.760A>G [p.Thr254Ala], and c.991C>T [p.Arg331Cys]) restored surface localization (Figure S5).

Discussion

The combination of the human genetic studies and cellular analysis of *GANAB*-null cells showed that

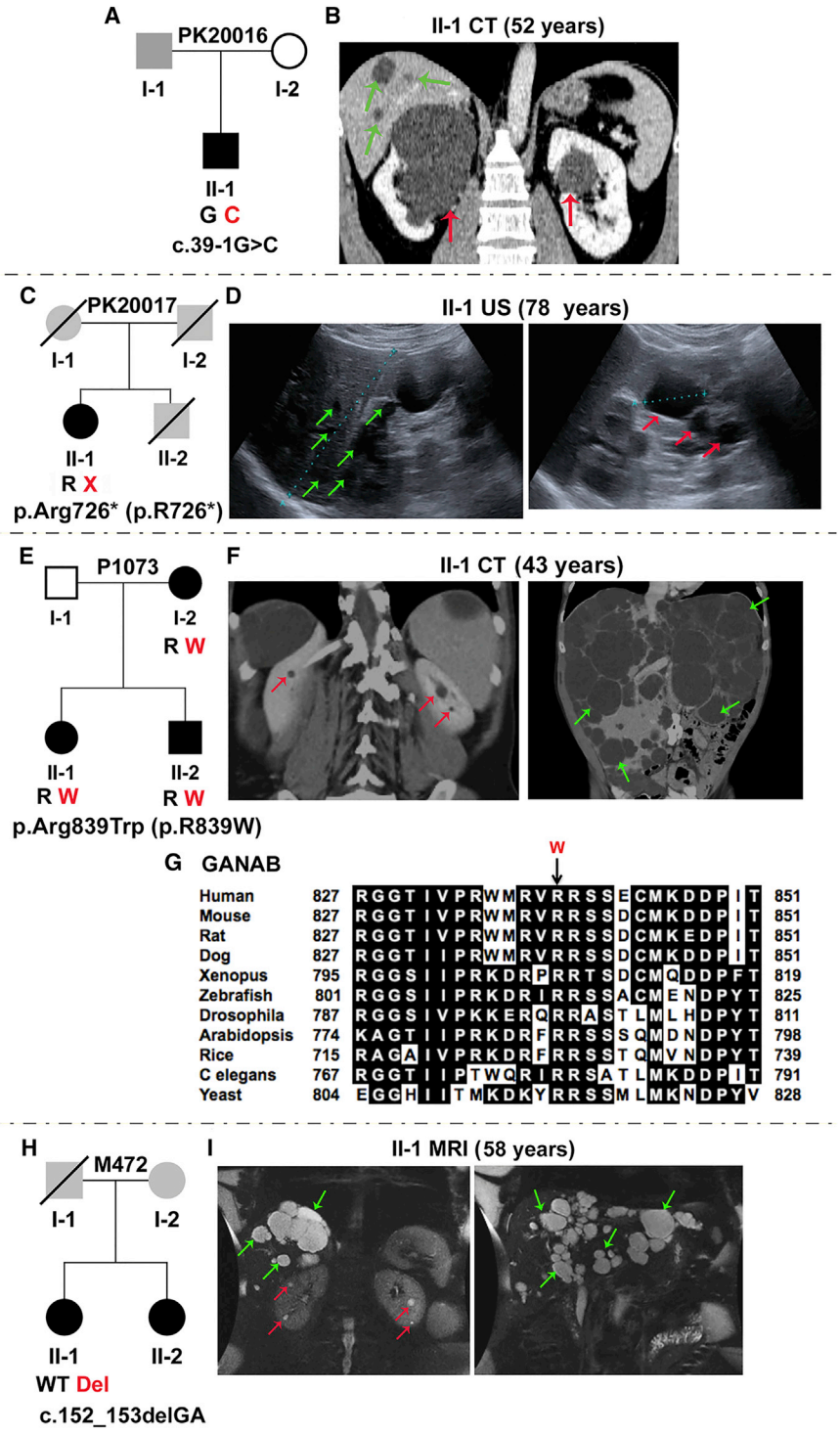

Figure 3. Characterization of *GANAB* Variants in Four Families, Including ADPLD-Affected P1073 and M472

(A) Pedigree of family PK20016 shows the splicing mutation c.39−1G>C (IVS1). The family history is unclear because samples were unavailable, but one large renal cyst was reported in I-1.

(B) CT scan of II-1 shows bilateral kidney cysts and occasional hepatic cysts.

(C) Pedigree of family PK20017 shows p.Arg726* (p.R726*) (c.2176C>T, exon 18), in the proband, II-1. A lack of DNA samples and clinical information precluded determining the family history. II-2 died at 55 years from a ruptured intracranial aneurysm, but his PKD status was unknown.

(D) Ultrasound examination of II-1 shows several liver (left), and kidney cysts (right).

(E) Pedigree of family P1073 shows p.Arg839Trp (p.R839W) (c.2515C>T, exon 22) in three affected individuals.

(F) CT scan of II-1 shows very few kidney cysts (left) but severe PLD (right). Gross images of the liver of this subject have been published.[57]

(G) MSA of *GANAB* (GIIα) orthologs shows invariant conservation of Arg839 across species. In silico mutation analysis highly predicts p.Arg839Trp (p.R839W) to be pathogenic (SIFT = 0.00, Align GVGD = C65).

(H) Pedigree of family M472 shows c.152_153delGA (p.Arg51Lysfs*21) (p.R51fs; exon 3) in II-1.

(I) MRI of II-1 shows a few renal cysts (left) but significant PLD; this image was subsequent to earlier resections (Table 1). No sample was available from II-2, but imaging also showed predominant PLD (Figure S3E). Unavailable parental DNA samples and limited clinical information precluded determining the family history, but I-1 was reported to have had a cerebral hemorrhage. Red and green arrows indicate kidney and liver cysts, respectively. Where multiple cysts are present, only representative cysts are highlighted.

mutations in *GANAB* cause ADPKD and ADPLD, that loss or reduction of GIIα is associated with maturation and localization defects of PC1 and PC2, and that the identified mutations cannot rescue the PC1 localization defect.

The renal phenotype associated with *GANAB* mutations is consistently mild without renal insufficiency, such that any kidney enlargement is due to a few large cysts. The phenotype caused by *GANAB* mutations is more similar to PKD2 than to PKD1 but is apparently even milder.[58] One individual had more severe PKD (M656 member II-3), and here an undetermined cystogenic influence from the mother might be significant. Applying imaging diagnostic criteria developed in PKD1- and PKD2-affected families[53,54] might be unreliable in families affected by *GANAB* mutations even in those with a largely renal phenotype given the disease mildness and the variability within families. The significance of the vascular disease, noted in families M641, PK20017, and M472, is presently unclear. Only in M641 do the definitely affected sisters have ICAs; the vascular phenotypes in three other individuals in these families are not proven to be linked to *GANAB* mutations.

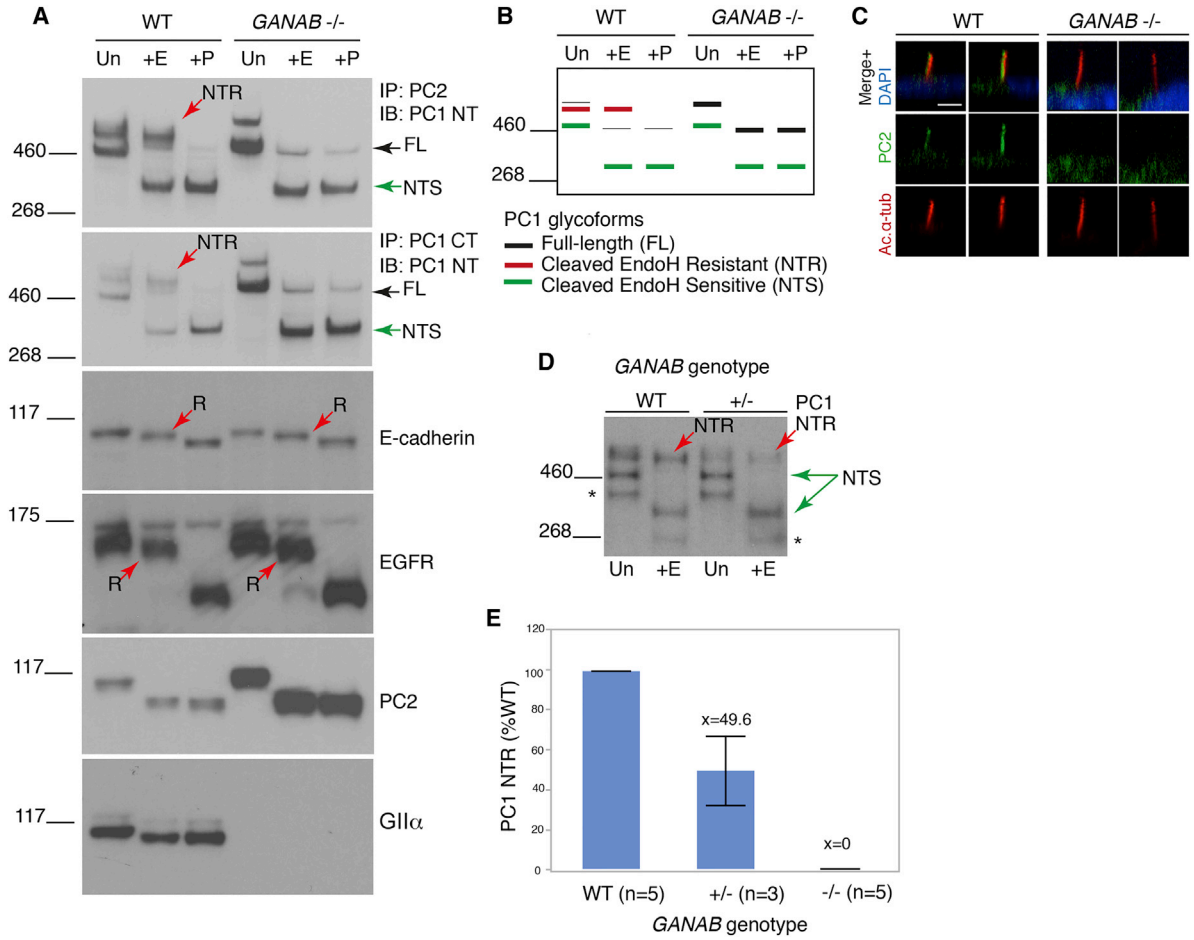

Figure 4. GIIα Is Required for PC1 ER Exit and Maturation

(A) Deglycosylation analysis of WT and *GANAB*$^{-/-}$ RCTE membrane protein either untreated (Un) or treated with EndoH (+E) or PNGaseF (+P). IP was used to enrich the PC1 complex with C-terminal PC1 (PC1-CT) or PC2 (YCE2) antibodies and immunodetected with the N-terminal PC1 (PC1-NT) antibody (7e12). Complete loss of the mature PC1 glycoform[15] (NTR; red arrow) was observed in *GANAB*$^{-/-}$ cells, and full-length PC1 (FL) and PC1-NTS became more abundant. Mature E-cadherin and EGFR were not or only marginally affected by *GANAB* loss; the EndoH-resistant protein (R, red arrow) persisted. No EndoH-resistant form of PC2 was noted,[15] but the protein was upregulated in *GANAB*$^{-/-}$ cells. Loss of WT GIIα was confirmed in *GANAB*$^{-/-}$ cells with the use of a C-terminal antibody.

(B) Schematic representation of the observed PC1 banding pattern in the WT and *GANAB*$^{-/-}$ cells shown in (A).

(C) Confocal z stack rendering of primary cilia in confluent WT and *GANAB*$^{-/-}$ cells in which acetylated α-tubulin (Ac.α-tub) and PC2 were detected shows no cilia PC2 signal in *GANAB*$^{-/-}$ cells. Nuclei were stained with DAPI, and 100 ciliated cells were analyzed in three independent experiments. The scale bar represents 10 μm.

(D) Immunoblot of PC1-NT in WT and *GANAB*$^{+/-}$ cells shows a reduced level of PC1-NTR in *GANAB*$^{+/-}$ cells. Asterisks indicate a non-specific product.[15]

(E) Quantification of PC1-NTR shows a reduction to ~50% ($p < 0.001$, Student's t test) in heterozygous cells and a complete loss in homozygous, *GANAB*$^{-/-}$ cells.

The liver disease is variable and ranges from no cysts to severe PLD requiring surgical intervention. The highly variable PLD phenotype is characteristic of ADPKD and ADPLD. Allelic effects do not appear to explain this variability, although some evidence of familial clustering of severe PLD suggests that genetic modifiers play a significant role.[25,46] It is interesting that *GANAB* mutations were identified as the cause of the disease in two of the seven ADPLD-affected families studied, suggesting that the mutation-detection rate might be higher in ADPLD-affected families. Although there might be ascertainment bias because ADPKD was the diagnosis in the vast majority of screened families, the overall phenotype appears to involve more renal disease than described in PRKCSH.[59] The reason for this is unclear given that they are subunits of the same protein, and further analysis of *GANAB* in ADPLD and *PRKCSH* in ADPKD populations is required. We show that phenotypes consistent with mild ADPKD and ADPLD involving a few renal cysts can be caused by *GANAB* mutations. Rather than considering ADPKD and ADPLD to be strictly separate diseases, we suggest recording the full range of phenotypes associated with each gene in which mutations are associated with ADPKD and/or ADPLD.

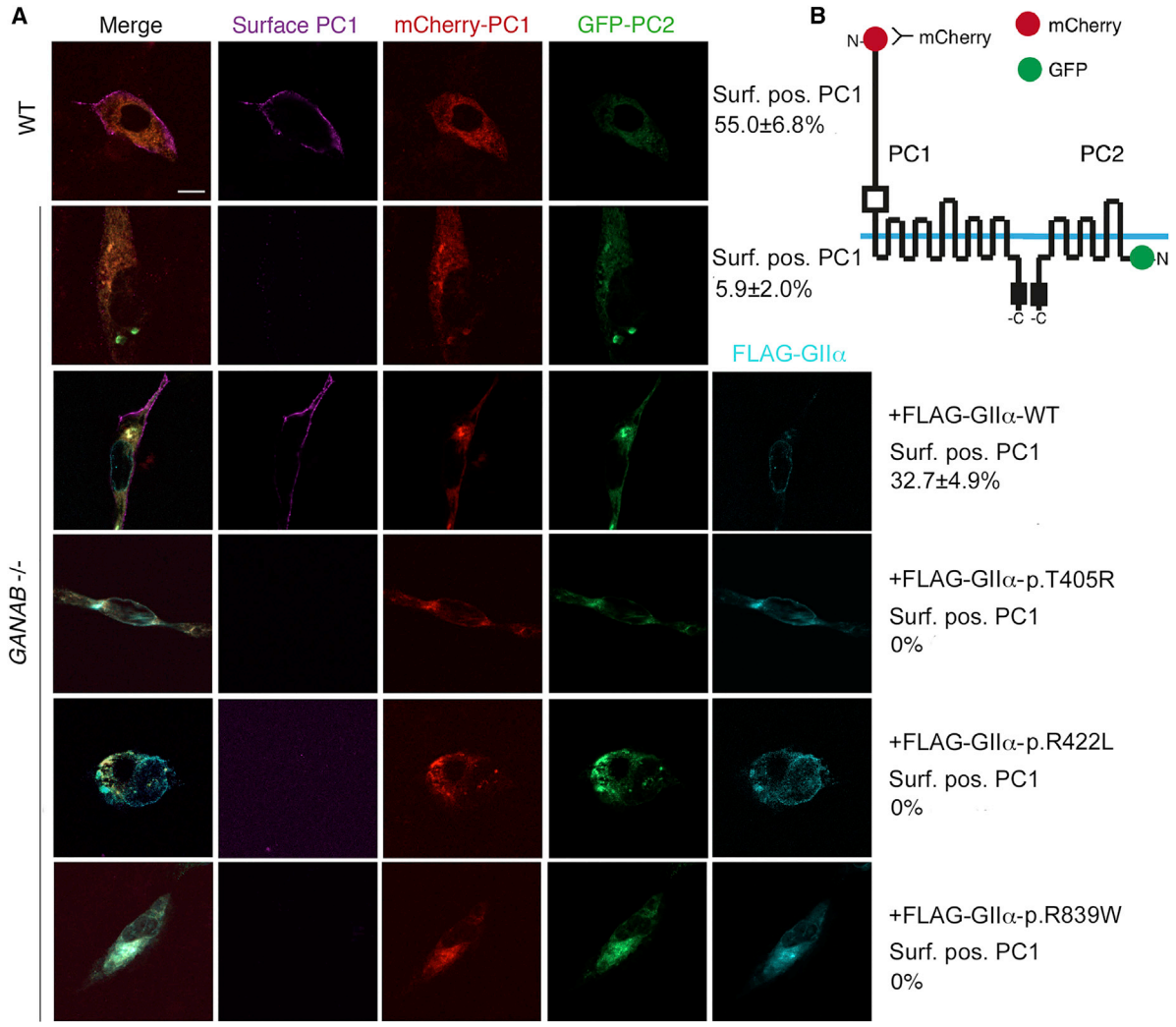

Figure 5. Surface Localization of PC1 Requires WT GIIα and Is Disrupted by *GANAB* Missense Mutations
(A) WT and $GANAB^{-/-}$ cells were co-transfected with WT tagged PC1 and PC2, mCherry-PC1, and TagGFP-PC2 and examined for surface mCherry-PC1 labeling. Co-transfected cells were screened for live cell-surface PC1 signal and quantified as the percentage of surface-positive PC1 cells out of the total co-transfected cells. Surface PC1 was detected on 55.0% ± 6.8% of WT cells but only 5.9% ± 2.0% of $GANAB^{-/-}$ cells ($p \leq 0.0001$), and the level was rescued to 32.7% ± 4.9% by co-transfection with the WT *GANAB* (FLAG-GIIα) plasmid. Co-transfection with the newly identified putative *GANAB* missense mutations cloned in FLAG-GIIα, p.Thr405Arg (p.T405R), p.Arg422Leu (p.R422L), and p.Arg839Trp (p.R839W) did not rescue PC1 surface localization (bottom three panels; all $p < 0.0001$ versus WT rescue). Student's t test was performed to determine significance in at least 100 triple-transfected cells analyzed among three independent experiments. The scale bar represents 20 μm.
(B) Diagram of the constructs.

GANAB mutations account for ~3% of GUR ADPKD-affected families (~0.3% total ADPKD), although given that many GUR cases most likely involve *PKD1* or *PKD2* mutations that were missed (see Introduction and Paul et al.[23]), they are probably responsible for a much greater proportion of missing genetic causes of ADPKD. In addition, because of the mild phenotype, these mutations are most likely underdiagnosed and, in particular, might be more common in families with mild PKD and significant PLD.

Defects in glycosylation and protein trafficking underlie a large number of human diseases,[60,61] but the interesting aspect here is the specificity of the phenotype associated with disruption of a step in a process important for many proteins. GII functions in the early cargo-recruitment steps of the calnexin and calreticulin cycle, which facilitates the quality control and maturation of transmembrane glycoproteins.[34] $GANAB^{-/-}$ cells and *S. pombe* mutants are viable without growth defects,[62,63] and we have demonstrated a lack of global, surface glycoprotein deficiencies in $GANAB^{-/-}$ cells, which suggests that endomannosidase activity and other chaperones and folding-assisting proteins can generally compensate for this loss, at least in non-stress conditions. The complexity due to protein size and extensive N-linked glycosylation might underlie the critical dependence of PC1 on GII and the calnexin and calreticulin cycle for achieving native folding. At this stage, it is unclear whether the enrichment of PLD associated with GII

deficiency indicates that the liver is particularly vulnerable to reduction of this enzyme. In contrast to that described for SEC63 deficiency,[15,62,64,65] the defect we observed in *GANAB*$^{-/-}$ cells was complete disruption of PC1 maturation, which increased ER accumulation of cleaved PC1 while only marginally affecting GPS cleavage. In RCTE cells, *GANAB* heterozygosity was associated with a ~50% reduction of PC1-NTR, a level predisposing to cyst development in association with stochastic, renal injury and/or somatic events.[12,15,66,67] However, fully understanding quantitatively how PC1 maturation is influenced by GII dosage will require further studies, which could provide insights into a therapeutic role for cellular and molecular chaperones in ADPKD.

Accession Numbers

The accession number for the cDNA sequence reported in this paper is GenBank: NM_198335.3.

Supplemental Data

Supplemental Data include five figures and three tables and can be found with this article online at http://dx.doi.org/10.1016/j.ajhg.2016.05.004.

Acknowledgments

We thank the families and coordinators for involvement in the study, the Exome Aggregation Consortium, Tatyana Masyuk, and other HALT Progression of Polycystic Kidney Disease (HALT-PKD) and Consortium for Radiologic Imaging Studies of Polycystic Kidney Disease (CRISP) investigators: Drs. Grantham, Yu, and Winklehofer (Kansas Medical Center), Bae, Abebe, and Landsittel (University of Pittsburgh), Schrier and Brosnahan (University of Colorado Denver), Perrone and Miskulin (Tufts University), Braun (Cleveland Clinic), Steinman (Beth Israel Deaconess Medical Center), Mrug (University of Alabama at Birmingham), Rahbari-Oskoui (Emory University), Bennett (Legacy Health, Portland), Flessner (National Institute of Diabetes and Digestive and Kidney Diseases [NIDDK]), Moore (Carolinas HealthCare, Charlotte), and Czarnecki (Brigham and Women's Hospital). This study received support from NIDDK grant DK058816, the Mayo PKD Translational Center (DK090728), an American Heart Association postdoctoral fellowship (B.P.), the Mayo Clinic Nephrology Training Grant (T32DK007013 to V.G.G.), an American Society of Nephrology (ASN) Foundation Kidney Research Fellowship (E.C.-L.G.) and Ben J. Lipps Research Fellowship (K.H.), the Mayo Graduate School (E.K.D.), the Zell Family Foundation, and Robert M. and Billie Kelley Pirnie. The CRISP and HALT-PKD studies were supported by NIDDK cooperative agreements (DK056943, DK056956, DK056957, DK056961, DK062410, DK062408, DK062402, DK082230, DK062411, and DK062401), National Center for Research Resources General Clinical Research Centers, and National Center for Advancing Translational Sciences Clinical and Translational Science Awards. The Genkyst cohort was supported by National Plans for Clinical Research, Groupement Interrégional de Recherche Clinique et d'Innovation (GIRCI Grand Ouest), and the French Society of Nephrology.

Received: February 16, 2016
Accepted: May 3, 2016
Published: June 2, 2016

Web Resources

ADPKD Mutation Database, http://pkdb.mayo.edu
Align GVGD, http://agvgd.iarc.fr
Berkeley *Drosophila* Genome Project NNSPLICE 0.9, http://www.fruitfly.org/seq_tools/splice.html
ExAC Browser, http://exac.broadinstitute.org
GeneReviews, Harris, P.C., and Torres, V.E. (2015). Polycystic Kidney Disease, Autosomal Dominant, http://www.ncbi.nlm.nih.gov/books/NBK1246/
GeneTests, https://www.genetests.org
NCBI Nucleotide, http://www.ncbi.nlm.nih.gov/nuccore
NHLBI Exome Sequencing Project (ESP) Exome Variant Server, http://evs.gs.washington.edu/EVS/
OMIM, http://www.omim.org
RefSeq, http://www.ncbi.nlm.nih.gov/refseq/
SIFT, http://sift.jcvi.org
UCSC Genome Browser, https://genome.ucsc.edu/

References

1. Torres, V.E., Harris, P.C., and Pirson, Y. (2007). Autosomal dominant polycystic kidney disease. Lancet *369*, 1287–1301.
2. Harris, P.C., and Torres, V.E. (2009). Polycystic kidney disease. Annu. Rev. Med. *60*, 321–337.
3. The European Polycystic Kidney Disease Consortium (1994). The polycystic kidney disease 1 gene encodes a 14 kb transcript and lies within a duplicated region on chromosome 16. Cell *77*, 881–894.
4. Mochizuki, T., Wu, G., Hayashi, T., Xenophontos, S.L., Veldhuisen, B., Saris, J.J., Reynolds, D.M., Cai, Y., Gabow, P.A., Pierides, A., et al. (1996). PKD2, a gene for polycystic kidney disease that encodes an integral membrane protein. Science *272*, 1339–1342.
5. Heyer, C.M., Sundsbak, J.L., Abebe, K.Z., Chapman, A.B., Torres, V.E., Grantham, J.J., Bae, K.T., Schrier, R.W., Perrone, R.D., Braun, W.E., et al.; HALT PKD and CRISP Investigators (2016). Predicted mutation strength of nontruncating PKD1 mutations aids genotype-phenotype correlations in autosomal dominant polycystic kidney disease. J. Am. Soc. Nephrol. Published online January 28, 2016. http://dx.doi.org/10.1681/ASN.2015050583.
6. Audrézet, M.P., Cornec-Le Gall, E., Chen, J.M., Redon, S., Quéré, I., Creff, J., Bénech, C., Maestri, S., Le Meur, Y., and Férec, C. (2012). Autosomal dominant polycystic kidney disease: comprehensive mutation analysis of PKD1 and PKD2 in 700 unrelated patients. Hum. Mutat. *33*, 1239–1250.
7. Cornec-Le Gall, E., Audrézet, M.P., Chen, J.M., Hourmant, M., Morin, M.P., Perrichot, R., Charasse, C., Whebe, B., Renaudineau, E., Jousset, P., et al. (2013). Type of PKD1 mutation influences renal outcome in ADPKD. J. Am. Soc. Nephrol. *24*, 1006–1013.
8. Grantham, J.J., Torres, V.E., Chapman, A.B., Guay-Woodford, L.M., Bae, K.T., King, B.F., Jr., Wetzel, L.H., Baumgarten, D.A., Kenney, P.J., Harris, P.C., et al.; CRISP Investigators (2006). Volume progression in polycystic kidney disease. N. Engl. J. Med. *354*, 2122–2130.

9. Ong, A.C., and Harris, P.C. (2015). A polycystin-centric view of cyst formation and disease: the polycystins revisited. Kidney Int. *88*, 699–710.
10. Qian, F., Boletta, A., Bhunia, A.K., Xu, H., Liu, L., Ahrabi, A.K., Watnick, T.J., Zhou, F., and Germino, G.G. (2002). Cleavage of polycystin-1 requires the receptor for egg jelly domain and is disrupted by human autosomal-dominant polycystic kidney disease 1-associated mutations. Proc. Natl. Acad. Sci. USA *99*, 16981–16986.
11. Wei, W., Hackmann, K., Xu, H., Germino, G., and Qian, F. (2007). Characterization of cis-autoproteolysis of polycystin-1, the product of human polycystic kidney disease 1 gene. J. Biol. Chem. *282*, 21729–21737.
12. Hopp, K., Ward, C.J., Hommerding, C.J., Nasr, S.H., Tuan, H.F., Gainullin, V.G., Rossetti, S., Torres, V.E., and Harris, P.C. (2012). Functional polycystin-1 dosage governs autosomal dominant polycystic kidney disease severity. J. Clin. Invest. *122*, 4257–4273.
13. Fedeles, S.V., Tian, X., Gallagher, A.R., Mitobe, M., Nishio, S., Lee, S.H., Cai, Y., Geng, L., Crews, C.M., and Somlo, S. (2011). A genetic interaction network of five genes for human polycystic kidney and liver diseases defines polycystin-1 as the central determinant of cyst formation. Nat. Genet. *43*, 639–647.
14. Kurbegovic, A., Kim, H., Xu, H., Yu, S., Cruanès, J., Maser, R.L., Boletta, A., Trudel, M., and Qian, F. (2014). Novel functional complexity of polycystin-1 by GPS cleavage in vivo: role in polycystic kidney disease. Mol. Cell. Biol. *34*, 3341–3353.
15. Gainullin, V.G., Hopp, K., Ward, C.J., Hommerding, C.J., and Harris, P.C. (2015). Polycystin-1 maturation requires polycystin-2 in a dose-dependent manner. J. Clin. Invest. *125*, 607–620.
16. Kim, H., Xu, H., Yao, Q., Li, W., Huang, Q., Outeda, P., Cebotaru, V., Chiaravalli, M., Boletta, A., Piontek, K., et al. (2014). Ciliary membrane proteins traffic through the Golgi via a Rabep1/GGA1/Arl3-dependent mechanism. Nat. Commun. *5*, 5482.
17. Rossetti, S., Consugar, M.B., Chapman, A.B., Torres, V.E., Guay-Woodford, L.M., Grantham, J.J., Bennett, W.M., Meyers, C.M., Walker, D.L., Bae, K., et al.; CRISP Consortium (2007). Comprehensive molecular diagnostics in autosomal dominant polycystic kidney disease. J. Am. Soc. Nephrol. *18*, 2143–2160.
18. Loftus, B.J., Kim, U.-J., Sneddon, V.P., Kalush, F., Brandon, R., Fuhrmann, J., Mason, T., Crosby, M.L., Barnstead, M., Cronin, L., et al. (1999). Genome duplications and other features in 12 Mb of DNA sequence from human chromosome 16p and 16q. Genomics *60*, 295–308.
19. Consugar, M.B., Wong, W.C., Lundquist, P.A., Rossetti, S., Kubly, V.J., Walker, D.L., Rangel, L.J., Aspinwall, R., Niaudet, W.P., Ozen, S., et al.; CRISP Consortium (2008). Characterization of large rearrangements in autosomal dominant polycystic kidney disease and the *PKD1/TSC2* contiguous gene syndrome. Kidney Int. *74*, 1468–1479.
20. Tan, A.Y., Blumenfeld, J., Michaeel, A., Donahue, S., Bobb, W., Parker, T., Levine, D., and Rennert, H. (2015). Autosomal dominant polycystic kidney disease caused by somatic and germline mosaicism. Clin. Genet. *87*, 373–377.
21. Heidet, L., Decramer, S., Pawtowski, A., Morinière, V., Bandin, F., Knebelmann, B., Lebre, A.S., Faguer, S., Guigonis, V., Antignac, C., and Salomon, R. (2010). Spectrum of *HNF1B* mutations in a large cohort of patients who harbor renal diseases. Clin. J. Am. Soc. Nephrol. *5*, 1079–1090.
22. Eckardt, K.U., Alper, S.L., Antignac, C., Bleyer, A.J., Chauveau, D., Dahan, K., Deltas, C., Hosking, A., Kmoch, S., Rampoldi, L., et al. (2015). Autosomal dominant tubulointerstitial kidney disease: diagnosis, classification, and management–A KDIGO consensus report. Kidney Int. *88*, 676–683.
23. Paul, B.M., Consugar, M.B., Ryan Lee, M., Sundsbak, J.L., Heyer, C.M., Rossetti, S., Kubly, V.J., Hopp, K., Torres, V.E., Coto, E., et al. (2014). Evidence of a third ADPKD locus is not supported by re-analysis of designated PKD3 families. Kidney Int. *85*, 383–392.
24. Pirson, Y., Chauveau, D., and Torres, V. (2002). Management of cerebral aneurysms in autosomal dominant polycystic kidney disease. J. Am. Soc. Nephrol. *13*, 269–276.
25. Chebib, F.T., Jung, Y., Heyer, C.M., Irazabal, M.V., Hogan, M.C., Harris, P.C., Torres, V.E., and El-Zoghby, Z.M. (2016). Effect of genotype on the severity and volume progression of polycystic liver disease in ADPKD. Nephrol. Dial. Transplant. Published online February 29, 2016. http://dx.doi.org/10.1093/ndt/gfw008.
26. Hogan, M.C., Abebe, K., Torres, V.E., Chapman, A.B., Bae, K.T., Tao, C., Sun, H., Perrone, R.D., Steinman, T.I., Braun, W., et al. (2015). Liver involvement in early autosomal-dominant polycystic kidney disease. Clin. Gastroenterol. Hepatol. *13*, 155–164.e6.
27. Hoevenaren, I.A., Wester, R., Schrier, R.W., McFann, K., Doctor, R.B., Drenth, J.P., and Everson, G.T. (2008). Polycystic liver: clinical characteristics of patients with isolated polycystic liver disease compared with patients with polycystic liver and autosomal dominant polycystic kidney disease. Liver Int. *28*, 264–270.
28. Drenth, J.P., te Morsche, R.H., Smink, R., Bonifacino, J.S., and Jansen, J.B. (2003). Germline mutations in *PRKCSH* are associated with autosomal dominant polycystic liver disease. Nat. Genet. *33*, 345–347.
29. Li, A., Davila, S., Furu, L., Qian, Q., Tian, X., Kamath, P.S., King, B.F., Torres, V.E., and Somlo, S. (2003). Mutations in *PRKCSH* cause isolated autosomal dominant polycystic liver disease. Am. J. Hum. Genet. *72*, 691–703.
30. Davila, S., Furu, L., Gharavi, A.G., Tian, X., Onoe, T., Qian, Q., Li, A., Cai, Y., Kamath, P.S., King, B.F., et al. (2004). Mutations in *SEC63* cause autosomal dominant polycystic liver disease. Nat. Genet. *36*, 575–577.
31. Cnossen, W.R., te Morsche, R.H., Hoischen, A., Gilissen, C., Chrispijn, M., Venselaar, H., Mehdi, S., Bergmann, C., Veltman, J.A., and Drenth, J.P. (2014). Whole-exome sequencing reveals LRP5 mutations and canonical Wnt signaling associated with hepatic cystogenesis. Proc. Natl. Acad. Sci. USA *111*, 5343–5348.
32. Sakai, K., Hirai, M., Minoshima, S., Kudoh, J., Fukuyama, R., and Shimizu, N. (1989). Isolation of cDNAs encoding a substrate for protein kinase C: nucleotide sequence and chromosomal mapping of the gene for a human 80K protein. Genomics *5*, 309–315.
33. Trombetta, E.S., Simons, J.F., and Helenius, A. (1996). Endoplasmic reticulum glucosidase II is composed of a catalytic subunit, conserved from yeast to mammals, and a tightly bound noncatalytic HDEL-containing subunit. J. Biol. Chem. *271*, 27509–27516.
34. Xu, C., and Ng, D.T. (2015). Glycosylation-directed quality control of protein folding. Nat. Rev. Mol. Cell Biol. *16*, 742–752.

35. D'Alessio, C., and Dahms, N.M. (2015). Glucosidase II and MRH-domain containing proteins in the secretory pathway. Curr. Protein Pept. Sci. *16*, 31–48.
36. Treml, K., Meimaroglou, D., Hentges, A., and Bause, E. (2000). The alpha- and beta-subunits are required for expression of catalytic activity in the hetero-dimeric glucosidase II complex from human liver. Glycobiology *10*, 493–502.
37. Tannous, A., Pisoni, G.B., Hebert, D.N., and Molinari, M. (2015). N-linked sugar-regulated protein folding and quality control in the ER. Semin. Cell Dev. Biol. *41*, 79–89.
38. Pelletier, M.F., Marcil, A., Sevigny, G., Jakob, C.A., Tessier, D.C., Chevet, E., Menard, R., Bergeron, J.J., and Thomas, D.Y. (2000). The heterodimeric structure of glucosidase II is required for its activity, solubility, and localization in vivo. Glycobiology *10*, 815–827.
39. Deprez, P., Gautschi, M., and Helenius, A. (2005). More than one glycan is needed for ER glucosidase II to allow entry of glycoproteins into the calnexin/calreticulin cycle. Mol. Cell *19*, 183–195.
40. Rothblatt, J.A., Deshaies, R.J., Sanders, S.L., Daum, G., and Schekman, R. (1989). Multiple genes are required for proper insertion of secretory proteins into the endoplasmic reticulum in yeast. J. Cell Biol. *109*, 2641–2652.
41. Sadler, I., Chiang, A., Kurihara, T., Rothblatt, J., Way, J., and Silver, P. (1989). A yeast gene important for protein assembly into the endoplasmic reticulum and the nucleus has homology to DnaJ, an Escherichia coli heat shock protein. J. Cell Biol. *109*, 2665–2675.
42. Deshaies, R.J., Sanders, S.L., Feldheim, D.A., and Schekman, R. (1991). Assembly of yeast Sec proteins involved in translocation into the endoplasmic reticulum into a membrane-bound multisubunit complex. Nature *349*, 806–808.
43. Skowronek, M.H., Rotter, M., and Haas, I.G. (1999). Molecular characterization of a novel mammalian DnaJ-like Sec63p homolog. Biol. Chem. *380*, 1133–1138.
44. Gao, H., Wang, Y., Wegierski, T., Skouloudaki, K., Pütz, M., Fu, X., Engel, C., Boehlke, C., Peng, H., Kuehn, E.W., et al. (2010). PRKCSH/80K-H, the protein mutated in polycystic liver disease, protects polycystin-2/TRPP2 against HERP-mediated degradation. Hum. Mol. Genet. *19*, 16–24.
45. Hofherr, A., Wagner, C., Fedeles, S., Somlo, S., and Köttgen, M. (2014). N-glycosylation determines the abundance of the transient receptor potential channel TRPP2. J. Biol. Chem. *289*, 14854–14867.
46. Waanders, E., te Morsche, R.H., de Man, R.A., Jansen, J.B., and Drenth, J.P. (2006). Extensive mutational analysis of PRKCSH and SEC63 broadens the spectrum of polycystic liver disease. Hum. Mutat. *27*, 830.
47. Kline, T.L., Korfiatis, P., Edwards, M.E., Warner, J.D., Irazabal, M.V., King, B.F., Torres, V.E., and Erickson, B.J. (2016). Automatic total kidney volume measurement on follow-up magnetic resonance images to facilitate monitoring of autosomal dominant polycystic kidney disease progression. Nephrol. Dial. Transplant. *31*, 241–248.
48. Cheong, B., Muthupillai, R., Rubin, M.F., and Flamm, S.D. (2007). Normal values for renal length and volume as measured by magnetic resonance imaging. Clin. J. Am. Soc. Nephrol. *2*, 38–45.
49. Levey, A.S., Stevens, L.A., Schmid, C.H., Zhang, Y.L., Castro, A.F., 3rd, Feldman, H.I., Kusek, J.W., Eggers, P., Van Lente, F., Greene, T., and Coresh, J.; CKD-EPI (Chronic Kidney Disease Epidemiology Collaboration) (2009). A new equation to estimate glomerular filtration rate. Ann. Intern. Med. *150*, 604–612.
50. Schwartz, G.J., Haycock, G.B., Edelmann, C.M., Jr., and Spitzer, A. (1976). A simple estimate of glomerular filtration rate in children derived from body length and plasma creatinine. Pediatrics *58*, 259–263.
51. Mashiko, D., Fujihara, Y., Satouh, Y., Miyata, H., Isotani, A., and Ikawa, M. (2013). Generation of mutant mice by pronuclear injection of circular plasmid expressing Cas9 and single guided RNA. Sci. Rep. *3*, 3355.
52. Ong, A.C.M., Harris, P.C., Davies, D.R., Pritchard, L., Rossetti, S., Biddolph, S., Vaux, D.J.T., Migone, N., and Ward, C.J. (1999). Polycystin-1 expression in PKD1, early-onset PKD1, and TSC2/PKD1 cystic tissue. Kidney Int. *56*, 1324–1333.
53. Pei, Y., Obaji, J., Dupuis, A., Paterson, A.D., Magistroni, R., Dicks, E., Parfrey, P., Cramer, B., Coto, E., Torra, R., et al. (2009). Unified criteria for ultrasonographic diagnosis of ADPKD. J. Am. Soc. Nephrol. *20*, 205–212.
54. Pei, Y., Hwang, Y.H., Conklin, J., Sundsbak, J.L., Heyer, C.M., Chan, W., Wang, K., He, N., Rattansingh, A., Atri, M., et al. (2015). Imaging-based diagnosis of autosomal dominant polycystic kidney disease. J. Am. Soc. Nephrol. *26*, 746–753.
55. (ExAC), E.A.C. (2016). Exome Aggregation Consortium (ExAC) Cambridge, MA (URL: http://exac.broadinstitute.org).
56. Lek, M., Karczewski, K., Minikel, E., Samocha, K., Banks, E., Fennell, T., O'Donnell-Luria, A., Ware, J., Hill, A., Cummings, B., et al. (2015). Analysis of protein-coding genetic variation in 60,706 humans. bioRxiv, http://dx.doi.org/10.1101/030338.
57. Urribarri, A.D., Munoz-Garrido, P., Perugorria, M.J., Erice, O., Merino-Azpitarte, M., Arbelaiz, A., Lozano, E., Hijona, E., Jiménez-Agüero, R., Fernandez-Barrena, M.G., et al. (2014). Inhibition of metalloprotease hyperactivity in cystic cholangiocytes halts the development of polycystic liver diseases. Gut *63*, 1658–1667.
58. Harris, P.C., Bae, K., Rossetti, S., Torres, V.E., Grantham, J.J., Chapman, A., Guay-Woodford, L., King, B.F., Wetzel, L.H., Baumgarten, D., et al. (2006). Cyst number but not the rate of cystic growth is associated with the mutated gene in autosomal dominant polycystic kidney disease. J. Am. Soc. Nephrol. *17*, 3013–3019.
59. Cnossen, W.R., and Drenth, J.P. (2014). Polycystic liver disease: an overview of pathogenesis, clinical manifestations and management. Orphanet J. Rare Dis. *9*, 69.
60. Hung, M.C., and Link, W. (2011). Protein localization in disease and therapy. J. Cell Sci. *124*, 3381–3392.
61. Hennet, T., and Cabalzar, J. (2015). Congenital disorders of glycosylation: a concise chart of glycocalyx dysfunction. Trends Biochem. Sci. *40*, 377–384.
62. D'Alessio, C., Fernández, F., Trombetta, E.S., and Parodi, A.J. (1999). Genetic evidence for the heterodimeric structure of glucosidase II. The effect of disrupting the subunit-encoding genes on glycoprotein folding. J. Biol. Chem. *274*, 25899–25905.
63. Reitman, M.L., Trowbridge, I.S., and Kornfeld, S. (1982). A lectin-resistant mouse lymphoma cell line is deficient in glucosidase II, a glycoprotein-processing enzyme. J. Biol. Chem. *257*, 10357–10363.
64. Fedeles, S.V., So, J.S., Shrikhande, A., Lee, S.H., Gallagher, A.R., Barkauskas, C.E., Somlo, S., and Lee, A.H. (2015). Sec63 and

Xbp1 regulate IRE1α activity and polycystic disease severity. J. Clin. Invest. *125*, 1955–1967.

65. Moore, S.E., and Spiro, R.G. (1990). Demonstration that Golgi endo-α-D-mannosidase provides a glucosidase-independent pathway for the formation of complex *N*-linked oligosaccharides of glycoproteins. J. Biol. Chem. *265*, 13104–13112.
66. Gallagher, A.R., Germino, G.G., and Somlo, S. (2010). Molecular advances in autosomal dominant polycystic kidney disease. Adv. Chronic Kidney Dis. *17*, 118–130.
67. Takakura, A., Contrino, L., Zhou, X., Bonventre, J.V., Sun, Y., Humphreys, B.D., and Zhou, J. (2009). Renal injury is a third hit promoting rapid development of adult polycystic kidney disease. Hum. Mol. Genet. *18*, 2523–2531.

The American Journal of Human Genetics, Volume *98*

Supplemental Data

Mutations in *GANAB*, Encoding the Glucosidase IIα Subunit, Cause Autosomal-Dominant Polycystic Kidney and Liver Disease

Binu Porath, Vladimir G. Gainullin, Emilie Cornec-Le Gall, Elizabeth K. Dillinger, Christina M. Heyer, Katharina Hopp, Marie E. Edwards, Charles D. Madsen, Sarah R. Mauritz, Carly J. Banks, Saurabh Baheti, Bharathi Reddy, José Ignacio Herrero, Jesús M. Bañales, Marie C. Hogan, Velibor Tasic, Terry J. Watnick, Arlene B. Chapman, Cécile Vigneau, Frédéric Lavainne, Marie-Pierre Audrézet, Claude Ferec, Yannick Le Meur, Vicente E. Torres, Genkyst Study Group, HALT Progression of Polycystic Kidney Disease Group, Consortium for Radiologic Imaging Studies of Polycystic Kidney Disease, and Peter C. Harris

SUPPLEMENTAL FIGURES

Figure S1

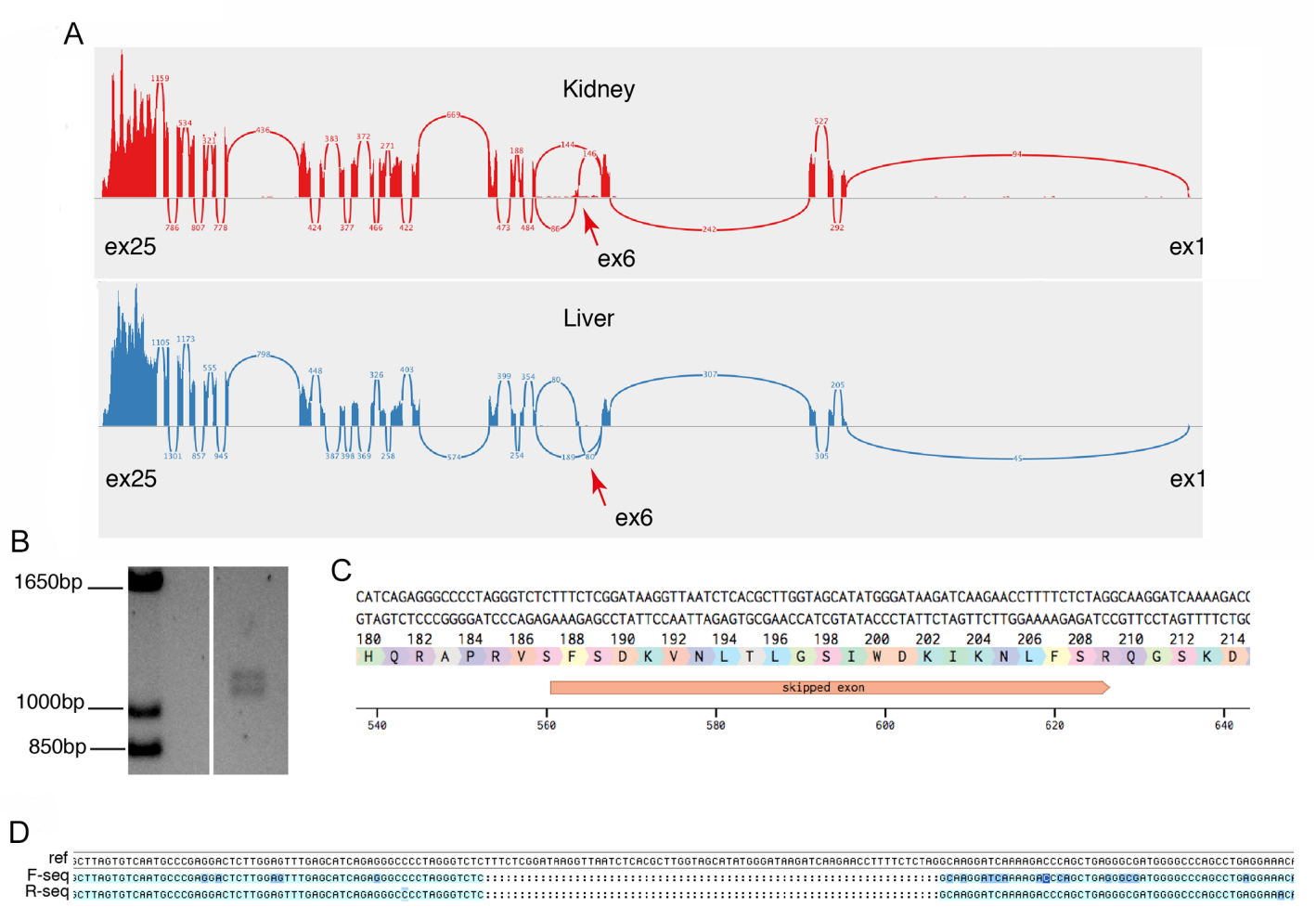

Figure S1: Analysis of *GANAB* isoforms. (**A**) Sashimi plots summarizing the results of the Illumina BodyMap 2.0 RNAseq data set (ENA archive: ERP000546) for *GANAB* mRNA expression in human liver and kidney tissue visualized using Integrated Genome Viewer (IGV, Broad Institute; 45 read threshold). Note in both liver and kidney the splice forms with (Isoform 3; NM_198335) and without exon 6 (Isoform 2; NM_198334) are approximately equally represented. (**B**) RT-PCR of RCTE cells showing two distinct products with primers flanking exon 6, which are confirmed by sequencing to be isoforms 3 and 2 (**D**). (**C**) Diagram showing the inframe exon 6 region (66bp, 22aa) skipped in isoform 2.

Figure S2

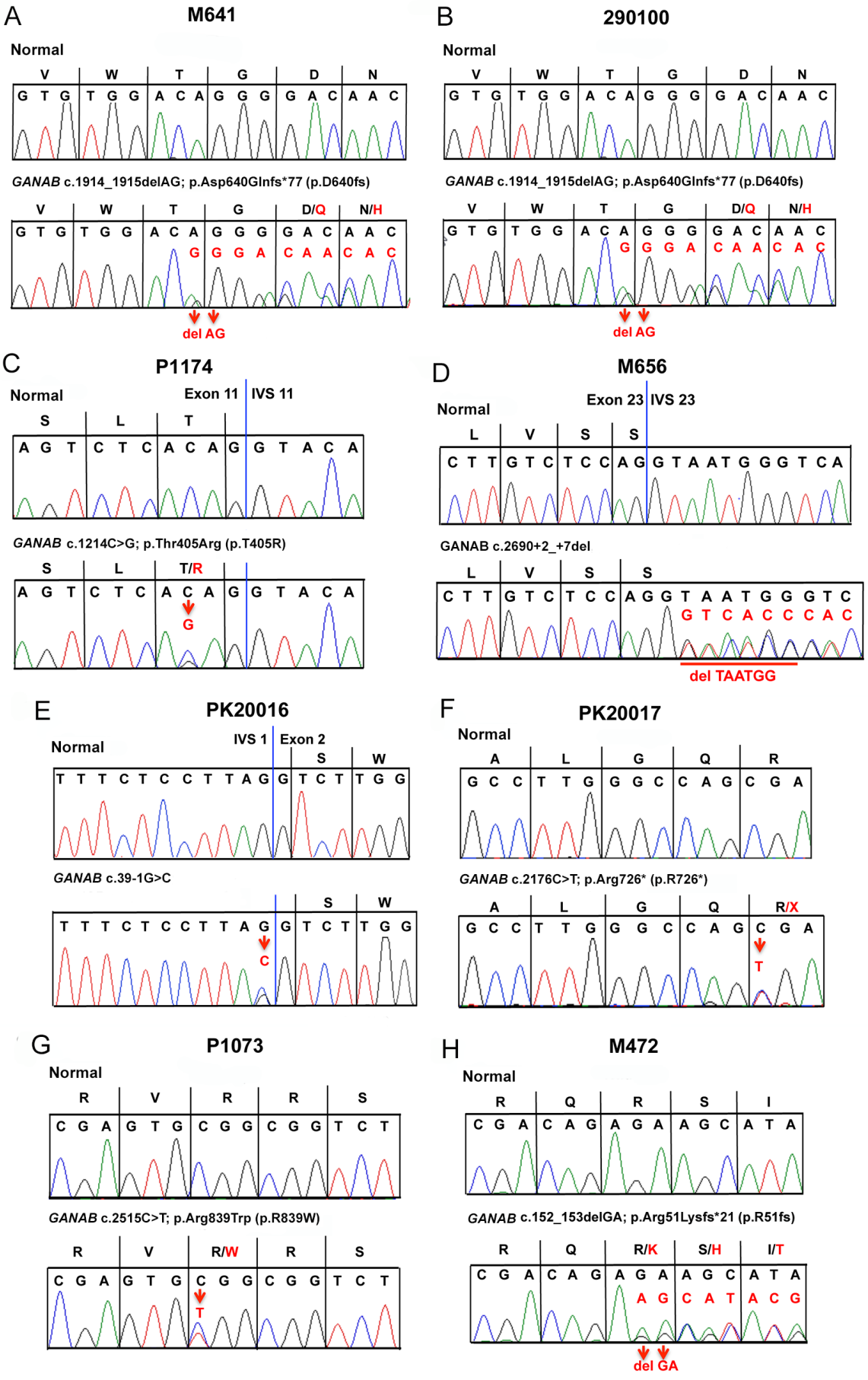
A
M641
Normal
V W T G D N
G T G T G G A C A G G G G A C A A C
GANAB c.1914_1915delAG; p.Asp640GInfs*77 (p.D640fs)
V W T G D/Q N/H
G T G T G G A C A G G G G A C A A C
G G G A C A A C
del AG
B
290100
Normal
V W T G D N
G T G T G G A C A G G G G A C A A C
GANAB c.1914_1915delAG; p.Asp640GInfs*77 (p.D640fs)
V W T G D/Q N/H
G T G T G G A C A G G G G A C A A C
G G G A C A A C
del AG
C
P1174
Normal
Exon 11 IVS 11
S L T
A G T C T C A C A G G T A C A
GANAB c.1214C>G; p.Thr405Arg (p.T405R)
S L T/R
A G T C T C A C A G G T A C A
G
D
M656
Exon 23 IVS 23
Normal
L V S S
C T T G T C T C C A G G T A A T G G G T C A
GANAB c.2690+2_+7del
L V S S
C T T G T C T C C A G G T A A T G G G T C
G T C A C C C A C
del TAATGG
E
PK20016
Normal
IVS 1 Exon 2
S W
T T T C T C C T T A G G T C T T G G
GANAB c.39-1G>C
S W
T T T C T C C T T A G G T C T T G G
C
F
PK20017
Normal
A L G Q R
G C C T T G G G C C A G C G A
GANAB c.2176C>T; p.Arg726* (p.R726*)
A L G Q R/X
G C C T T G G G C C A G C G A
T
G
P1073
Normal
R V R R S
C G A G T G C G G C G G T C T
GANAB c.2515C>T; p.Arg839Trp (p.R839W)
R V R/W R S
C G A G T G C G G C G G T C T
T
H
M472
Normal
R Q R S I
C G A C A G A G A A G C A T A
GANAB c.152_153delGA; p.Arg51Lysfs*21 (p.R51fs)
R Q R/K S/H I/T
C G A C A G A G A A G C A T A
A G C A T A C G
del GA

Figure S2: Sequence of *GANAB* mutations detected by Sanger sequencing in eight families. (**A**) M641, c.1914_1915delAG; p.Asp640Glnfs*77 (p.D640fs), (**B**) 290100, c.1914_1915delAG; p.Asp640Glnfs*77 (p.D640fs), (**C**) P1174, c.1214C>G; pThr405Arg (p.T405R), (**D**) M656, c2690+2_+7del, (**E**) PK20016, c.39-1G>C, (**F**) PK20017, c.2176C>T; p.Arg726* (p.R726*), (**G**) P1073, c.2515C>T; p.Arg839Trp (p.R839W), (**H**) M472, c.152_153delGA; p.Arg51Lysfs*21 (p.R51fs). Each component figure shows the sequence of the specific *GANAB* variant indicated in red (bottom panel), compared to the normal sequence (top panel). Note that the deletion in M656 disrupts the canonical donor site. The substitution in P1174 is close to end of exon 11 but is not predicted to alter splicing.

Figure S3

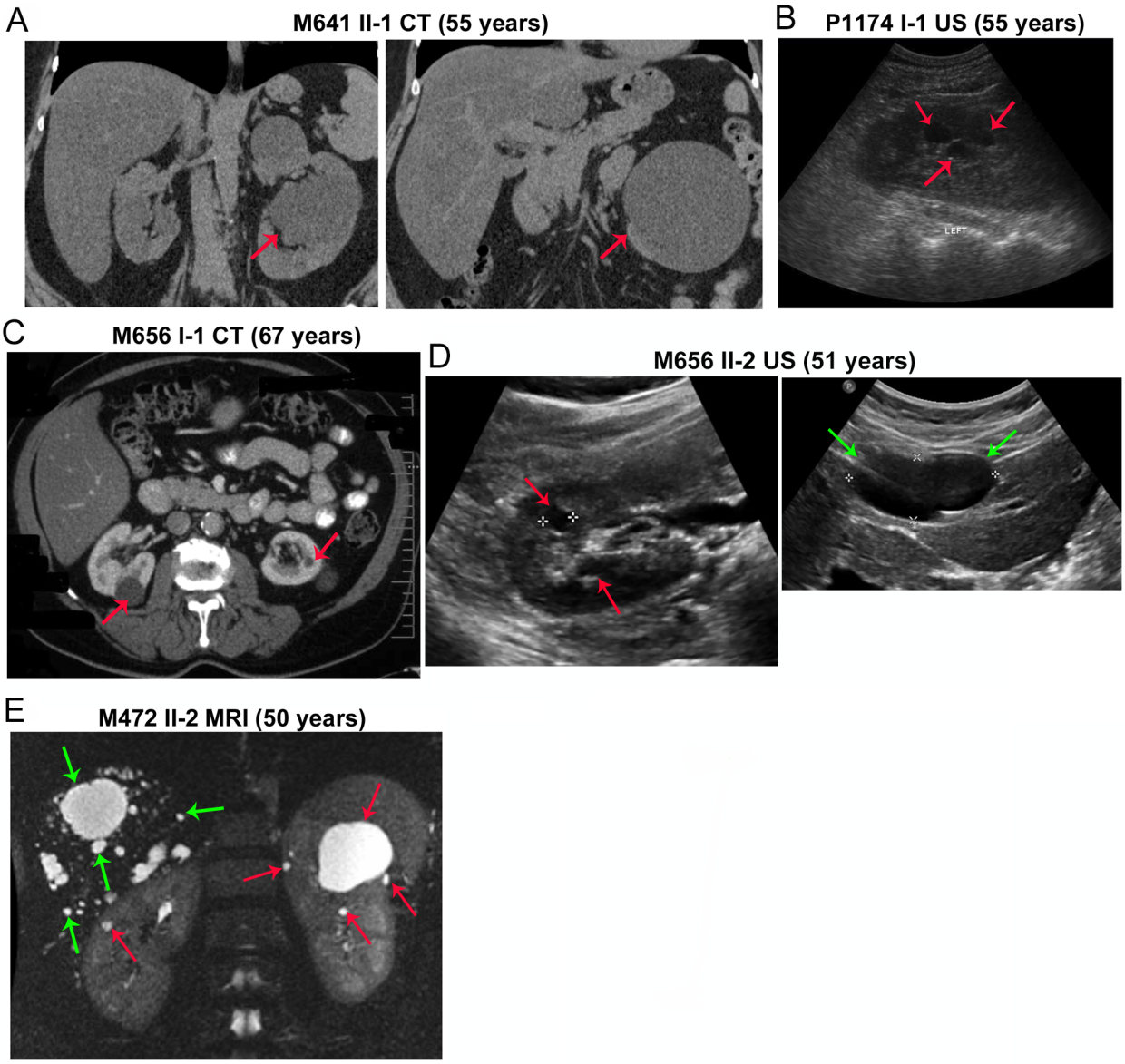

Figure S3: Kidney and liver images from affected members of families with *GANAB* mutations. Kidney and liver cysts are indicated with red or green arrows, respectively. Just representative cysts are highlighted where multiple cysts are present. (**A**) CT scan without contrast of kidneys and liver from M641, II-1 at 55y showing several kidney cysts, including a large one causing organ enlargement. Liver cysts are not evident in this image without contrast and organ enlargement may be due to fatty infiltrate (Table 1). (**B**) US image of kidneys from P1174, I-1 at 55y showing three moderately sized cysts. (**C**) CT scan image with contrast from M656, I-1 at 67y showing a few kidney cysts, but no apparent liver cysts. (**D**) Ultrasound of M656, II-2 at 51y showing a few renal cysts (left) and two large liver cysts (right). (**E**) T2-weighted MRI images from M472, II-2 at 50y showing a few renal cysts and multiple scattered liver cysts.

Figure S4

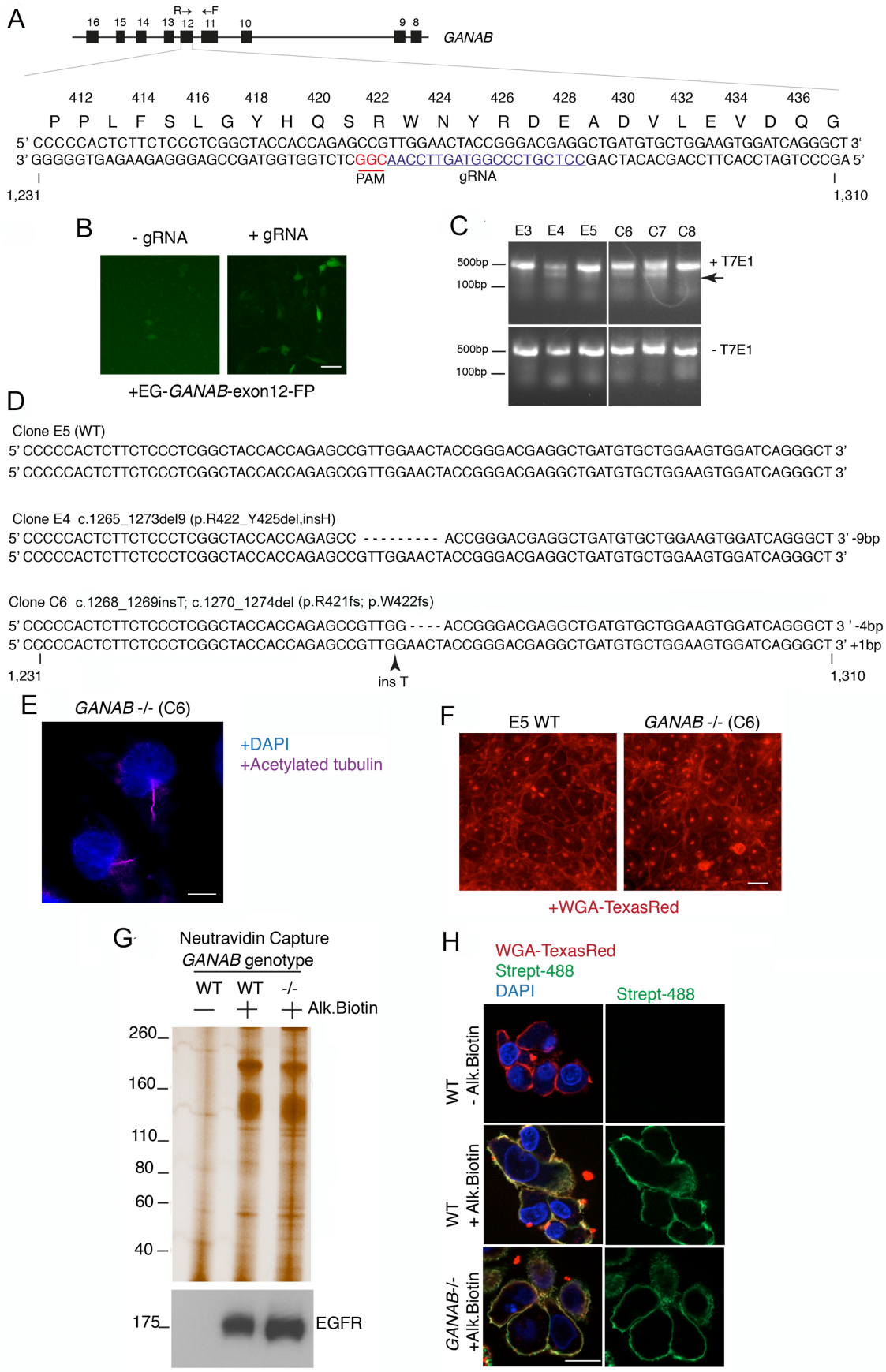
A
R→ ←F
16 15 14 13 12 11 10 9 8
GANAB
412 414 416 418 420 422 424 426 428 430 432 434 436
P P L F S L G Y H Q S R W N Y R D E A D V L E V D Q G
5' CCCCCACTCTTCTCCCTCGGCTACCACCAGAGCCGTTGGAACTACCGGGACGAGGCTGATGTGCTGGAAGTGGATCAGGGCT 3'
3' GGGGGTGAGAAGAGGGAGCCGATGGTGGTCTCGGCAACCTTGATGGCCCTGCTCCGACTACACGACCTTCACCTAGTCCCGA 5'
PAM
gRNA
1,231
1,310
B
- gRNA
+ gRNA
+EG-GANAB-exon12-FP
C
E3 E4 E5 C6 C7 C8
500bp
100bp
+ T7E1
- T7E1
D
Clone E5 (WT)
5' CCCCCACTCTTCTCCCTCGGCTACCACCAGAGCCGTTGGAACTACCGGGACGAGGCTGATGTGCTGGAAGTGGATCAGGGCT 3'
5' CCCCCACTCTTCTCCCTCGGCTACCACCAGAGCCGTTGGAACTACCGGGACGAGGCTGATGTGCTGGAAGTGGATCAGGGCT 3'
Clone E4 c.1265_1273del9 (p.R422_Y425del,insH)
5' CCCCCACTCTTCTCCCTCGGCTACCACCAGAGCC --------- ACCGGGACGAGGCTGATGTGCTGGAAGTGGATCAGGGCT 3' -9bp
5' CCCCCACTCTTCTCCCTCGGCTACCACCAGAGCCGTTGGAACTACCGGGACGAGGCTGATGTGCTGGAAGTGGATCAGGGCT 3'
Clone C6 c.1268_1269insT; c.1270_1274del (p.R421fs; p.W422fs)
5' CCCCCACTCTTCTCCCTCGGCTACCACCAGAGCCGTTGG - - - - ACCGGGACGAGGCTGATGTGCTGGAAGTGGATCAGGGCT 3 ' -4bp
5' CCCCCACTCTTCTCCCTCGGCTACCACCAGAGCCGTTGGAACTACCGGGACGAGGCTGATGTGCTGGAAGTGGATCAGGGCT 3' +1bp
ins T
1,231
1,310
E
GANAB -/- (C6)
+DAPI
+Acetylated tubulin
F
E5 WT
GANAB -/- (C6)
+WGA-TexasRed
G
Neutravidin Capture
GANAB genotype
WT WT -/-
Alk.Biotin
260
160
110
80
60
40
175
EGFR
H
WGA-TexasRed
Strept-488
DAPI
Strept-488
WT - Alk.Biotin
WT + Alk.Biotin
GANAB-/- +Alk.Biotin

Figure S4: Generation and characterization of RCTE cells with targeted *GANAB* deletion using the CRISPR/Cas9 system. (**A**) Diagram of *GANAB* showing the targeted region and sequence plus the position of the employed gRNA and protospacer adjacent motif (PAM). (**B**) Testing of the *GANAB* exon 12 gRNA using targeted sequence flanked by two halves of EGFP (EGxxFP)[1], EG-*GANAB*_exon12-FP. Cas9/gRNA co-transfected with EG-GANAB_exon12-FP in RCTE cells promotes recombination and EGFP fluorescence in transfected cells (Bar = 100μm). (**C**) PCR of a 550bp genomic region including *GANAB* exon 12 showing digestion due to mismatched sequence in clones E4, C6 and C7 (arrow) following T7E1 treatment. (**D**) DNA sequencing showing the inframe deletion in clone E4 and biallelic, frameshifting mutations in clone C6. (**E**) Confluent *GANAB*$^{-/-}$ RCTE cells detected with acetylated α-tubulin and stained with DAPI showing that they form normal cilia. Bar = 10μm. (**F**) Wheat Germ Agglutinin (WGA), which reacts with mature surface sugars, staining of WT and *GANAB*$^{-/-}$ RCTE clones shows similar staining, indicating no gross terminal glycosylation defects. (**G**) Biotinylation of terminally processed sialylated sugars with alkoxyamine biotin (Alk. Biotin) and neutravidin capture followed by silver staining showing similar surface glycoprotein detection in WT and *GANAB*$^{-/-}$ RCTE cells. (**H**) Cells employed for neutravidin capture (**G**), detected with WGA and streptavidin-488 to confirm surface glycoprotein labeling specificity. Scale bar = 20μm.

Figure S5

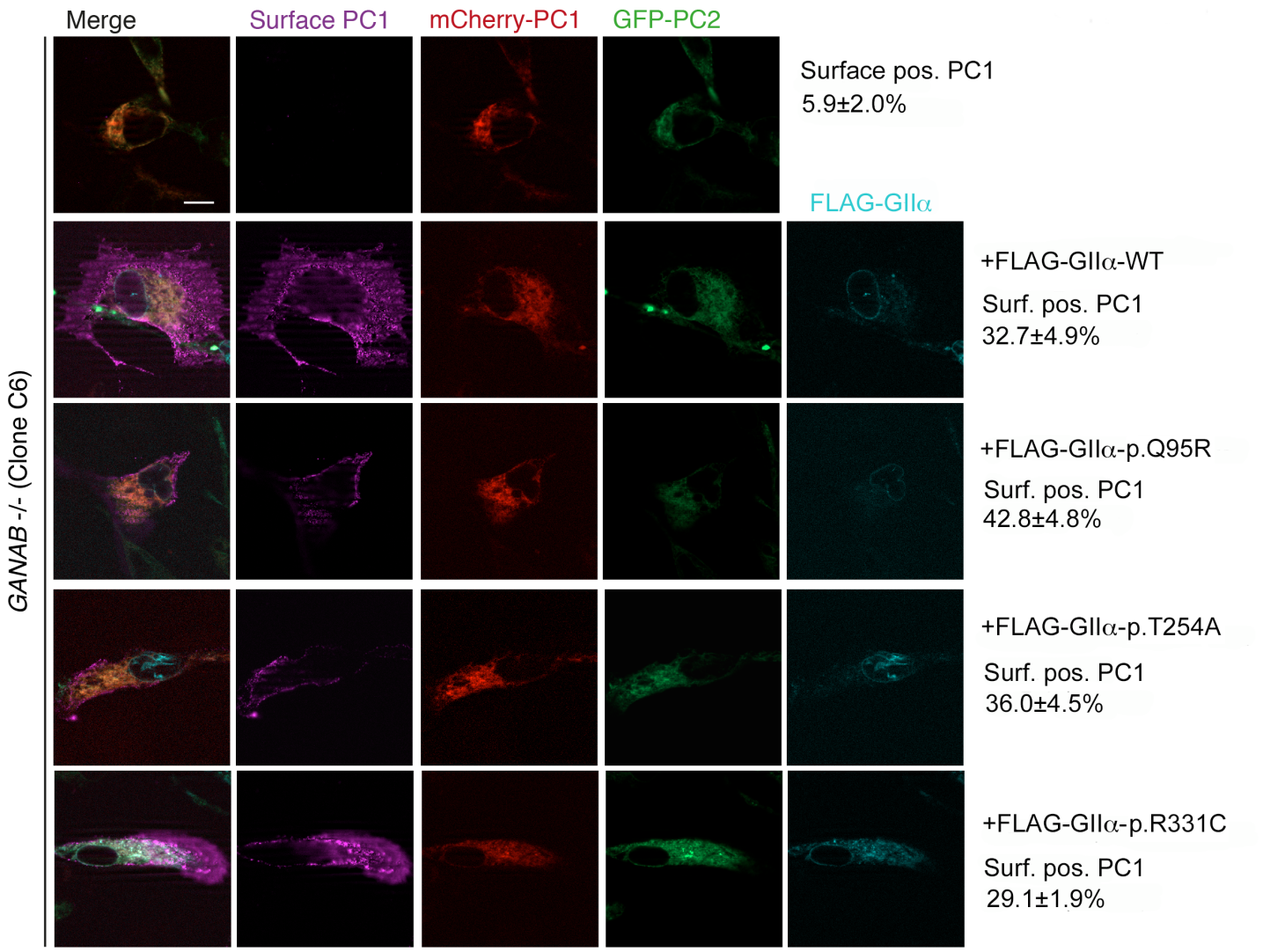

Figure S5: Surface localization of PC1 tested in *GANAB*$^{-/-}$ cells transfected with GIIα variants. Three *GANAB* missense variants either poorly predicted to be pathogenic from bioinformatics analysis (p.Gln95Arg [p.Q95R] and p.Thr254Ala [p.T254A]) or that are commonly found in the ExAC server (p.Arg331Cys [p.R331C]) were assayed for surface localization of PC1. *GANAB*$^{-/-}$ RCTE cells were co-transfected with mCherry-PC1 and GFP-PC2 as well as FLAG tagged GIIα plasmids that are WT (+FLAG-GIIα-WT) or contain the variants and examined for live-cell surface mCherry-PC1. In triple transfected *GANAB*$^{-/-}$ cells, p.Gln95Arg (p.Q95R; P=0.1), p.Thr254Ala (p.T254A; P=0.6), and p.Arg331Cys (p.R331C; P=0.5) were not significantly different from WT in their able to rescue PC1 surface localization, indicating that they are likely neutral variants. Students T-test was performed to determine significance in at least 100 triple-transfected cells analyzed between three independent experiments. Scale bar=20μm.

Table S1: Identified possible pathogenic variants detected by whole exome sequencing

Family[1]	Chr.	Position	Gene	Transcript	Exon	HGVS Coding	HGVS Protein	#Passed Filters[2]
P75	5	66438330	MAST4	NM_001164664	21	c.2699A>C	p.Q900P	5
	5	131940620	RAD50	NM_005732	16	c.2647C>T	p.R883C	5
	8	25261105	DOCK5	NM_024940	48	c.4958G>A	p.R1653H	5
	11	66328939	ACTN3	NM_001104	17	c.2006G>A	p.R672Q	5
	16	10867236	TVP23A	NM_001079512	5	c.387A>G	p.I129M	5
	19	49364918	PLEKHA4	NM_020904	4	c.224G>A	p.R75H	5
M199	4	190876287	FRG1	NM_004477	5	c.413G>A	p.W138*	6
	12	50598436	LIMA1	NM_001113546	6	c.763C>T	p.R255*	6
	12	51773085	GALNT6	NM_007210	3	c.481C>T	p.R161*	6
	14	64676186	SYNE2	NM_182914	102	c.18430G>A	p.D6144N	6
	16	2376215	ABCA3	NM_001089	5	c.115C>T	p.L39F	6
	1	22448067	WNT4	NM_030761	3	c.316A>G	p.T106A	5
	4	190876272	FRG1	NM_004477	5	c.398G>A	p.G133E	5
	6	12161747	HIVEP1	NM_002114	8	c.6563A>G	p.N2188S	5
	12	14927737	H2AFJ	NM_177925	1	c.333C>G	p.N111K	5
M263	1	26887275	RPS6KA1	NM_001006665	14	c.1301G>A	p.G434D	6
	2	215798885	ABCA12	NM_173076	52	c.7597G>A	p.A2533T	6
	3	120449574	RABL3	NM_173825	2	c.107C>A	p.S36*	6
	3	128694748	KIAA1257	NM_020741	7	c.897-2A>G	p.W300fs	6
	4	190876287	FRG1	NM_004477	5	c.413G>A	p.W138*	6
	9	35102108	STOML2	NM_013442	3	c.267G>T	p.Q89H	6
	11[3]	**62398260**	**GANAB**	**NM_198335**	**12**	**c.1265G>T**	**p.R422L**	**6**
	11	67377897	NDUFV1	NM_007103	5	c.556G>C	p.A186P	6
	12	106820980	POLR3B	NM_018082	13	c.1107A>T	p.L369F	6
	13	25671369	PABPC3	NM_030979	1	c.1033G>T	p.E345*	6
	15	90934098	IQGAP1	NM_003870	2	c.148G>A	p.A50T	6
	17	21319792	KCNJ12	NM_021012	3	c.1138G>A	p.E380K	6
	19	8322803	CERS4	NM_024552	10	c.782G>T	p.C261F	6
	22	18613671	TUBA8	NM_018943	5	c.1118G>A	p.R373Q	6
	2	152293802	RIF1	NM_018151	13	c.1420C>A	p.H474N	5
	2	233655546	GIGYF2	NM_001103147	12	c.917G>C	p.S306T	5
	3	49761081	GMPPB	NM_013334	1	c.79G>C	p.D27H	5
	4	190876272	FRG1	NM_004477	5	c.398G>A	p.G133E	5
	5	149782705	CD74	NM_001025159	7	c.796C>T	p.R266C	5
	8	144688809	PYCRL	NM_023078	4	c.413A>G	p.N138S	5
	9	101980978	ALG2	NM_033087	2	c.489G>C	p.E163D	5
	10	26446251	MYO3A	NM_017433	26	c.2806G>A	p.D936N	5
	11	1017041	MUC6	NM_005961	31	c.5760C>A	p.Y1920*	5
	11	1477645	BRSK2	NM_001256627	17	c.1736G>T	p.G579V	5
	12	53647451	MFSD5	NM_001170790	2	c.1153G>A	p.G385R	5
	14	23311809	MMP14	NM_004995	4	c.571C>A	p.P191T	5
	14	105613735	JAG2	NM_002226	20	c.2407A>T	p.I803F	5
	17	65944369	BPTF	NM_182641	23	c.7873G>A	p.E2625K	5
M560	1	1572296	CDK11B	NM_033487	14	c.995T>A	p.L332Q	6
	3	1337405	CNTN6	NM_014461	6	c.575G>A	p.G192D	6
	16[4]	2140803	PKD1	NM_001009944	44	c.12010C>T	p.Q4004*	6
	1	236228234	NID1	NM_002508	1	c.146G>A	p.G49E	5
	2	170042319	LRP2	NM_004525	50	c.9539C>T	p.P3180L	5

	2	179431879	TTN	NM_001267550	326	c.78980G>A	p.R26327Q	5
	5	78977820	PAPD4	NM_001114394	14	c.1316C>T	p.T439I	5
	13	52532497	ATP7B	NM_000053	8	c.2305A>G	p.M769V	5
	18	11889468	MPPE1	NM_023075	5	c.412C>T	p.R138W	5
	21	33711066	URB1	NM_014825	26	c.4460C>T	p.P1487L	5
	21	34889894	GART	NM_000819	15	c.1724C>T	p.P575L	5
P907	1	21903087	ALPL	NM_000478	11	c.1262A>G	p.Y421C	6
	1	24706274	STPG1	NM_001199013	5	c.331G>A	p.A111T	6
	2	170072887	LRP2	NM_004525	35	c.5702C>T	p.A1901V	6
	7	7495725	COL28A1	NM_001037763	16	c.1321G>A	p.G441R	6
	7	141759383	MGAM	NM_004668	32	c.3931C>T	p.R1311W	6
	11	18048098	TPH1	NM_004179	6	c.742C>T	p.R248*	6
	14	102749873	MOK	NM_014226	2	c.64C>T	p.Q22*	6
	15	78882221	CHRNA5	NM_000745	5	c.488C>T	p.P163L	6
	1	43032040	CCDC30	NM_001080850	6	c.749G>T	p.R250L	5
	1	145273300	NOTCH2NL	NM_203458	3	c.154C>T	p.R52*	5
	2	172931008	METAP1D	NM_199227	5	c.514G>A	p.G172R	5
	5	33596160	ADAMTS12	NM_030955	17	c.2533C>T	p.R845C	5
	5	140166534	PCDHA1	NM_018900	1	c.659C>A	p.P220Q	5
	5	140222006	PCDHA8	NM_018911	1	c.1100C>T	p.T367I	5
	11	65631296	MUS81	NM_025128	10	c.983T>C	p.L328P	5
	15	34649630	NUTM1	NM_001284292	8	c.3421C>T	p.R1141C	5
	16	23208666	SCNN1G	NM_001039	6	c.995A>G	p.H332R	5
	17	74005483	EVPL	NM_001988	22	c.3803G>A	p.R1268H	5
	22	50886828	SBF1	NM_002972	38	c.5197C>T	p.R1733C	5
P1272	1	93998617	FNBP1L	NM_001164473	8	c.778G>A	p.E260K	5
	1	216166437	USH2A	NM_206933	35	c.6730G>A	p.V2244M	5
	2	190922360	MSTN	NM_005259	3	c.752C>T	p.P251L	5
	2	197706020	PGAP1	NM_024989	27	c.2707T>C	p.Y903H	5
	3	160783259	PPM1L	NM_139245	3	c.643G>A	p.G215R	5
	5	13752253	DNAH5	NM_001369	64	c.11018C>T	p.S3673F	5
	12	104144483	STAB2	NM_017564	60	c.6565G>A	p.D2189N	5
	20	54824351	MC3R	NM_019888	1	c.452G>A	p.R151H	5

1: Details of subjects screened per family
P75 5 members screened: 3 affected siblings, 1 unaffected sibling, and unaffected mother
M199 3 members screened: 3 affected, maternal uncle and 2 nieces
M263 2 members screened: 2 affected, father and daughter
M560 3 members screened: 3 affected, mother and 2 daughters
P907 3 members screened: 2 affected daughters and an unaffected mother
P1272 2 members screened: 2 affected, maternal grandfather and grandchild
2: Only variants listed are those considered likely neutral by ≤ 1/6 programs, with the number of programs predicting pathogenicity listed (see Online Methods for details)
3: *GANAB* mutation is bolded
4: *PKD1* mutation missed by Sanger sequencing detected in this family

Table S2: Details of CRISPR/Cas9 guide RNA sequences

Name	DNA Sequence
gRNA1	TGCCTCATTCTTCTGCTCTT
gRNA2	CGGCAATATGCTAGTCTCAC
gRNA3	CCAGAGCCGTTGGAACTACC
gRNA4	CCTCGTCCCGGTAGTTCCAA
gRNA5	TGTGATGTCATCTGGCTAGA

Table S3: Details of primer sequences for generating site directed mutations

Mutation	Forward sequence	Reverse sequence
c.284A>G; p.Gly95Arg	CAGGGGCTTCgAAAGAACATG	AAGCTCTAGCACCAGCAAC
c.760A>G; p.Thr254Ala	GACATTCAAAgCTCACTCTGACAGCAAGC	TCCTCCCAGGCTCCTGGC
c.991C>T; p.Arg331Cys	CAACCCTCATtGCGACTTGGG	TGTGCCAGGAGCACAGGC
c.1214 C>G; p.Thr405Arg	GCTAGTCTCAgAGGAACCCAG	ATATTGCCGGAAAACATCAG
c.1265 G>T; p.Arg422Leu	CACCAGAGCCtTTGGAACTAC	GTAGCCGAGGGAGAAGAG
c. 2515 C>T; p.Arg839Trp	TGCGAGTGtGGCGGTCTTCAG	TCCATCGAGGCACGATTGT

REFERENCE

1. Mashiko, D. *et al.* Generation of mutant mice by pronuclear injection of circular plasmid expressing Cas9 and single guided RNA. *Sci Rep* **3**, 3355 (2013).